Prion cross-seeding between fungal and mammalian amyloid signaling motifs

Thierry Bardin[1], Asen Daskalov[1,], Sophie Barrouilhet[1#a], Alexandra Granger-Farbos[1], Bénédicte Salin[1], Corinne Blancard[1], Sven J. Saupe[1*] and Virginie Coustou[1*]

[1] Non-Self Recognition in Fungi, Institut de Biochimie et de Génétique Cellulaire (CNRS UMR 5095, Université de Bordeaux), 33077 Bordeaux, France.

[#a] Current Address: Universite de Pau et des Pays de l'Adour, E2S UPPA, CNRS, IPREM UMR 5254, Hélioparc, 64053 Pau, France

*Corresponding authors

E-mail : virginie.coustou@ibgc.cnrs.fr (VC); sven.saupe@ibgc.cnrs.fr (SJS)

Running title: Amyloid signaling pathways in *P. anserina*

Key words: amyloid; prion; programmed cell death; RHIM; RIP1, RIP3

Abstract

In fungi, NLR-based signalosomes activate downstream membrane-targeting cell-death inducing proteins by a mechanism of amyloid templating. In the species *Podospora anserina*, two such signalosomes, NWD2/HET-S and FNT1/HELLF have been described as well as an analogous system, involving a distinct amyloid signaling motif termed PP in the species *Chaetomium globosum*. The PP-motif bears resemblance to the RHIM and RHIM-like motifs controlling necroptosis in mammals and innate immunity in Drosophila. We identified here, a third NLR signalosome in *Podospora anserina* comprising a PP-motif and organized as a two-gene cluster encoding a NLR and a HELL-domain cell-death execution protein termed HELLP. We show that the PP-motif region of HELLP forms a prions we term [π] and that [π] prions trigger the cell-death inducing activity of full length HELLP. We detect no prion cross-seeding between HET-S, HELLF and HELLP amyloid motifs. In addition, we find that akin to PP-motifs, RHIM motifs from human RIP1 and RIP3 kinases are able to form prions in Podospora, and that [π] and [Rhim] prions cross-seed. Our study shows Podospora display three independent amyloid signalosomes. Based on the described functional similarity between RHIM and PP it appears likely that these amyloid motifs constitute evolutionary related cell-death signaling modules.

Author summary

Amyloids are fibrillar protein polymers assembled from cross β-sheets. Pathogenic amyloids are responsible for a range of neuronal and systemic protein misfolding diseases. In addition, functional amyloids fulfill a variety of biological functions in microbes and animals. In fungi, amyloids control prion-like signaling pathways with roles in host defense and immune

programmed cell death. These signaling pathways involve a Nod-like receptor and a cell-death execution protein activated through amyloid templating. In *P. anserina* two such amyloid signaling systems were identified so far. Here we identified and characterized a third amyloid signaling system comprising a different amyloid motif termed PP. We showed a total absence of cross-induction between the three *P. anserina* systems allowing for the co-existence of three independent amyloid signaling cascades in the same organism. An evolutionary relationship between fungal amyloid motifs and mammalian RHIM amyloid motif involved in the necroptosis pathway was previously suggested. We validated this assumption by showing that the human RHIM motif could not only propagate as a prion in *P. anserina* but also functionally cross-interact with the fungal PP-motif prions. These results point to a long term evolutionary conservation of amyloid signaling mechanisms from fungi to mammals.

52 # Introduction

53 Prions are protein polymers that behave as infectious entities by propagating their amyloid
54 structural state [1,2]. In addition to disease causing prions in mammals, prions have been
55 identified in fungi as infectious, cytoplasmic, non-Mendelian genetic elements [3]. One such
56 prion is [Het-s] of the filamentous fungus *Podospora anserina.* [Het-s] functions in a non-self
57 recognition process known as heterokaryon incompatibility. The *het-s* gene exists as two
58 incompatible allelic variants termed *het-s* and *het-S*. The HET-s protein when assembled into
59 the self-propagating prion form confers incompatibility to the HET-S variant, meaning that co-
60 expression of the [Het-s] prion with HET-S leads to cell death. The soluble non-prion form
61 confers a phenotype termed [Het-s*] compatible with HET-S [4,5]. [Het-s*] strains acquire the
62 prion state either spontaneously at a low frequency or systematically after fusion with a prion
63 infected strain. HET-s and HET-S are highly homologous allelic variants that display two
64 domains, a C-terminal Prion-Forming Domain (PFD) necessary and sufficient for prion
65 propagation and a N-terminal α-helical globular domain named HeLo responsible for cell-
66 death inducing activity [6,7]. The HET-s PFD is natively unfolded in the soluble state and upon
67 prion formation assembles into to a specific cross-β amyloid structure [6,8–10]. The HET-s β-
68 solenoid fold is composed of 2 rungs of β-strands per monomer, comprising two 21 residues
69 imperfect repeats (R1 and R2) connected by a flexible loop [9,11]. In [Het-s]/HET-S
70 incompatibility cell death is triggered when the [Het-s] PFD templates conversion of the HET-
71 S PFD region into the β-solenoid fold which in turn induces refolding of the HET-S HeLo domain
72 that acquires pore-forming activity by exposing an N-terminal transmembrane helix targeting
73 the cell membrane [7,12]. In this incompatibility system, HET-S acts as cell-death execution
74 protein and [Het-s] triggers its activation.

75 Further work on the [Het-s] system revealed that this incompatibility system is
76 evolutionary derived from a programmed cell death pathway in which HET-S is activated by a
77 specific NLR receptor [13]. NLR receptors are intracellular receptors that control immune
78 defense and programmed cell death pathways in animals and plants and also in fungi and
79 function by ligand induced oligomerization [14,15]. The NWD2 NLR receptor is encoded by the
80 gene immediately adjacent to *het-S* in the *P. anserina* genome and displays a central NACHT
81 nucleotide binding and oligomerization domain and a C-terminal WD40 repeat domain. The
82 N-terminal region of NWD2 displays a short region of homology to the R1 and R2 motifs of
83 HET-s. This region designated R0 is able to adopt a *het-s*-like fold. Ligand induced
84 oligomerization of NWD2 allows for spatial clustering of R0 motifs, cooperative nucleation of
85 the β-solenoid fold templating activation of the HET-S HeLo domain [13,16,17]. More
86 generally, it is proposed that a fraction of the NLR receptors in fungi activate their cognate
87 effector domains by a mechanism of prion amyloid templating by which the amyloid fold
88 formed after oligomerization of the NLR receptor is transmitted through heterotypic
89 interactions to the amyloid motif found in the C-terminal of the effector protein [18].
90 NWD2/HET-S pair was used as a paradigm for extensive bioinformatic screening to identify
91 additional NLR/effector pairs functioning through amyloid templating in fungi [16,19]. This
92 search resulted in the identification in *Podospora anserina* of a distant homolog of HET-S
93 termed HELLF [20]. HELLF encodes a protein with a HeLo-like N-terminal domain and a C-
94 terminal PFD with two repeated submotifs that share less than 15% identity to the HET-s PFD.
95 The HeLo-like domain shows distant homology to the HET-S HeLo domain but also to the 4HB
96 pore-forming domain of the MLKL protein [21], the terminal effector protein of necroptotic
97 death in mammals, which led to the proposition that this form of fungal programmed cell
98 death is related to mammalian necroptosis [22]. The gene adjacent to *hellf* encodes a NLR with

99 a NB-ARC domain and TPR repeats termed FNT1, which bears a N-terminal R0 region
100 homologous to the HELLF R1 and R2 PFD repeats. HELLF behaves analogously to HET-S in every
101 aspect that was analyzed. The C-terminal region of HELLF forms a prion termed [Φ] and [Φ] is
102 incompatible with full length HELLF. Upon interaction with [Φ], HELLF relocates to cell
103 membrane region and causes cell death and the N-terminal region of FNT1 forms fibrils and is
104 able to induce [Φ] prion formation. The solid-state NMR structure of the HELLF PFD structure
105 revealed that HET-s and HELLF prions have an almost identical backbone structure in spite of
106 extensive sequence divergence. The FNT1/HELLF system thus constitutes a second cell death-
107 inducing amyloid signaling pathway of *Podospora anserina*. Noteworthy is the fact that in spite
108 of their almost identical backbone structure [Het-s] and [Φ] prions do not cross-seed
109 indicating that NWD2/HET-S and FNT1/HELLF constitute two parallel signaling pathways.

110 In bioinformatics surveys, additional amyloid signaling motifs were identified in fungi
111 [14,16]. In particular, a prion motif termed PP (and also associated to NLR signaling) was
112 characterized in *Chaetomium globosum* in a three-gene cluster. In this case, the NLR protein
113 PNT1 regulates activation of two effector proteins, a HeLo-like domain cell death inducing
114 protein, HELLP (herein renamed CgHELLP for clarity) and a putative lipase, SBP. Remarkably,
115 the PP-motif is related in sequence to the RHIM amyloid motif that controls assembly of the
116 RIP1 and RIP3 kinases in the necroptosis pathway in mammals [13,22,23]. RHIM-like amyloid
117 motifs also occurs in the PGRP-LC, PGRP-LE, and Imd proteins controlling anti-bacterial
118 immunity in Drosophila [24]. The structure of the mammalian RIP1-RIP3 core (forming an
119 hetero-amyloid signaling complex) has recently been established [25]. RHIM amyloids
120 comprise two protein units per cross-β layer that run antiparallel and are interdigitated in a
121 compact hydrophobic interface formed by the G-(I,V)-Q-(I,V)-G motif. This central core motif
122 is common to the PP-motif but structural characterization of PP-amyloids will be required to

123 determine whether this short sequence homology reflect structural similarity between RHIM
124 and PP-amyloids.
125 Herein, we mine the genome of *P. anserina* and identify HELLP, a novel protein PP-motif
126 protein that defines a third cell death inducing amyloid signaling pathway in that species. We
127 show that the C-terminal PP-motif of HELLP forms a prion termed [π] in *Podospora anserina*
128 and assembles into fibrils *in vitro.* We find that akin to HET-S and HELLF, membrane-targeting
129 cell death inducing activity of HELLP can be triggered by [π] prions or by the prion form of the
130 N-terminal region of the HELLP-associated NLR, termed PNT1. We analyze in *Podospora*
131 *anserina* the functional interactions of the HET-s, HELLF and HELLP PFD prions and find that
132 they form three independent signaling systems. We further analyze prion formation by
133 mammalian RHIM motifs and find that [Rhim] and [π] prions partially cross-seed underlying
134 the functional similarity between these mammalian and fungal amyloid motifs.
135

136 # Results

137 ## A PP-motif gene cluster in *Podospora anserina*

138 During the course of a survey of NLR encoding genes in fungi, we identified, in *Podospora*
139 *anserina* a gene (*Pa_5_8060*) encoding a NLR with a NB-ARC domain and TPR repeats (we term
140 PNT1) [14]. We found that the adjacent gene (*Pa_5_8070*) encodes a HeLo-like-domain (HELL)
141 protein, we term HELLP (Fig 1A). HELLP shows homology to the CgHELLP cell-death execution
142 protein of *Chaetomium globosum* (Fig 1B and S1 Fig) [22]. As previously reported for CgHELLP
143 and HELLF, the HELL domain of HELLP shows homology to the 4HB membrane-targeting
144 domain of the mammalian MLKL necroptosis execution protein (S1 Fig). The N-terminal region
145 of PNT1 and the C-terminal region of HELLP share a region of homology encompassing a

146 predicted PP amyloid motif (Fig 1B) [22]. This region is also homologous to the RHIM motif
147 found in the RIP1 and RIP3 kinase in humans [23,25]. Based on the homology between HELLP
148 and CgHELLP, we reasoned that analogously to *nwd2/het-s* and *fnt1/hellf*, the *pnt1/hellp* gene
149 pair might encode the components of a third amyloid NLR signalosome in Podospora (Fig 1A).
150 We thus engaged into the functional characterization of this gene cluster.
151

152 **The C-terminal region of HELLP is a prion-forming domain**

153 In order to analyze whether the C-terminal region of HELLP displays the anticipated prion
154 forming ability, we generated different constructs with the C-terminal domain of HELLP (214-
155 271) fused either to GFP or RFP (in a C-terminal position) or to GFP in an N-terminal position.
156 These constructs were expressed in a *Δhellp* strain of *P. anserina.* For all constructs, the
157 fluorescence signal was initially diffuse but cytoplasmic foci formed upon further growth
158 (Table 1 and Fig 2A). The number of transformants spontaneously exhibiting the foci
159 phenotype was determined after 5, 11 and 19 days of growth (Table 1). The highest rate of
160 spontaneous foci formation was observed for the fusion protein bearing the GFP in N-terminal
161 position. For all fusion constructs, strains with diffuse fluorescence were systematically
162 converted to the foci phenotype after cytoplasmic contact with strains expressing foci,
163 indicating that the foci state is transmitted by cytoplasmic contact and infectious. By analogy
164 with the [Het-s] system, we term the phenotypic state with diffuse fluorescence [π*] and the
165 foci state [π] (Fig 2A). We conclude from these experiments that the PP-motif region of
166 HELLP(214-271) allows for prion formation and propagation. As previously described for [Het-
167 s] [26], the [π] state could be reversed to [π*] in meiotic progeny. When a [π] strain is used as
168 male parent, the meiotic progeny display the [π*] phenotype.

169 The same experiments were also carried out with a larger construct HELLP(171-271) fused
170 to GFP either in N- or C-terminus (S2A Fig). The larger construct also led to foci formation but
171 in contrast to analogous HET-S and CgHELLP constructs (HET-S(157-289)-GFP and
172 CgHELLP(170-278)-GFP), HELLP(171-271) fusions did not form elongated aggregates [22,27].
173 HELLP(214-271) PFD region was expressed in *E. coli* with a C-terminal histidine tag and
174 purified under denaturing conditions. Upon removal of the denaturant by dialysis, the protein
175 spontaneously formed fibrils that most often associated laterally as bundles (Fig 2B). These
176 results indicate that the HELLP(214-271) PFD region is able to form fibrils *in vitro.*
177
178 **Table 1. Rate of spontaneous prion formation and propagation**

transgene(s)	days after transfection								
	5			11			19		
	Soluble	Aggregated		Soluble	Aggregated		Soluble	Aggregated	
	n	n	%	n	n	%	n	n	%
HELLP(214-271)-RFP	27	7	20.6	13	21	61.8	2	32	94.1
HELLP(214-271)-GFP	40	7	14.9	24	23	48.9	8	39	83.0
GFP-HELLP(214-271)	11	22	66.7	1	32	97.0	0	33	100.0
RIP3(444-469)-RFP	18	21	53.8	8	31	79.5	2	37	94.9
RIP3(444-469)-GFP	30	16	34.8	15	31	67.4	4	42	91.3
GFP-RIP3(524-551)	8	17	68.0	3	22	88.0	0	25	100.0
RIP1(524-551)-RFP	23	3	11.5	14	12	46.2	10	16	61.5
RIP1(524-551)-GFP	27	0	0.0	25	2	7.4	23	4	14.8
GFP-RIP1(524-551)	38	0	0.0	36	2	5.3	35	3	7.9

179
180

181 **HELLP relocates to the cell membrane and triggers cell death upon interaction**

182 **with [π] prions**

183 It was shown that HET-S, HELLF and CgHELLP cell-death inducing activity is induced by
184 interaction with the prion form of their respective PFDs [7,12,20,22]. As a result confrontation
185 of strains expressing PFDs in the prion state with strains expressing the corresponding full
186 length protein leads to an incompatibility reaction which results in the death of the fusion cells
187 [20,22,27]. This reaction manifests through the formation of a demarcation line visible at the
188 macroscopic level and termed "barrage". To determine whether HELLP could also lead to
189 incompatibility, strains expressing GFP-HELLP(214-271) were confronted to strains expressing
190 full length HELLP, either from the wild-type resident copy or from HELLP-GFP or HELLP-RFP
191 transgene copies in a *Δhellp* background (Fig 3A). A barrage reaction was observed specifically
192 in confrontations with strains expressing the [π] phenotype. [π*] strains did not produce a
193 barrage reaction. The barrage reaction was stronger with strains expressing HELLP-GFP or -
194 RFP fusions from the strong *gpd* promoter than with strains expressing HELLP from the
195 resident copy (Fig 3A).

196 Propagation of the [π] phenotype was then assayed using barrage test as typically done
197 for monitoring [Het-s] propagation. Upon previous contact with [π] strains, [π*] strains
198 became capable of forming a barrage with strains expressing full length HELLP (S1 Table and
199 S2 Fig). Based on these experiments the definition of the [π] phenotype can be expanded to
200 represent both the foci state of the PP-motif GFP and RFP fusions and the ability to produce a
201 barrage reaction to full-length HELLP. The [π*]/[π] phenotypes of HELLP(214-271) are in that
202 sense analogous to [Het-s*]/[Het-s] phenotypes of HET-s and [Φ*]/[Φ] phenotypes of
203 HELLF(209-277).

204 It was shown that prion conversion of the HET-S PFD leads to the refolding of the HET-S
205 HeLo domain that acquires pore-forming activity by exposing its N-terminal transmembrane
206 helix, relocating it to the cell membrane and inducing cell death [7,12]. The same relocalization
207 process was observed for HELLF and CgHELLP in the incompatibility reaction leading to cell
208 death [20,22]. We thus determined whether HELLP relocates to the cell membrane upon
209 interaction with [π] prions. We examined the contact zone between incompatible [π] and
210 HELLP-GFP or -RFP expressing strains (Fig 3B). While full length HELLP-GFP or -RFP alone
211 produced diffuse fluorescence signals that remain stable over time (S3 Fig), in fusion cells co-
212 expressing these proteins and the prion form of HELLP(214-271)-RFP or GFP-HELLP(214-271),
213 we observed a localization of HELLP at the cell membrane region. This localization is associated
214 to cell death as observed using the vital dye Evans Blue (Fig 3C). These observations indicate
215 that HELLP functions analogously to HET-S, HELLF and CgHELLP and that the HELL membrane-
216 targeting domain is regulated by prion conversion of the C-terminal PFD region.
217

218 **The PNT1(1-31) region forms a prion and induces HELLP activation**

219 It has been shown that the N-terminal region of NWD2 adopts an amyloid fold, displays prion
220 infectivity and is able to activate HET-S pore forming activity [13]. Similarly, N-terminal regions
221 of the FNT1 and CgPNT1 NLRs display prion forming activity and trigger the cell-death inducing
222 activity of their effectors proteins, HELLF and CgHELLP respectively [22]. To determine
223 whether the N-terminal region of PNT1 displays similar properties we expressed PNT1(1-31)
224 fused to GFP or RFP in *Δhellp* strains. Two phenotypic states were observed, a diffuse
225 cytoplasmic fluorescence state, and foci state comparable to the [π∗] and [π] phenotypes
226 observed previously with HELLP(214-271) (Fig 4A). Spontaneous conversion to the aggregated

227 form occurred after few days and cytoplasmic contact with [π] strains induced systematic
228 conversion.

229 PNT1(1-31)-GFP [π] strains systematically convert [π*] HELLP(214-271)-RFP strains to the
230 [π] state. Conversely, [π] HELLP(214-271)-RFP systematically convert [π*] PNT1(1-31)-GFP to
231 the [π] state.

232 PNT1(1-31) and HELLP(214-271) were then co-expressed in the same strain (Fig 4B).
233 Diffuse fluorescence was observed very briefly in the case of HELLP(214-271)-RFP and PNT1(1-
234 31)-GFP co-expression, indicating that these two proteins were in a soluble state just after
235 transfection. Then, dot-like aggregates formed concomitantly for the two proteins and co-
236 localized in the cell, as expected if they could interact and cross-seed *in vivo*. The same was
237 true during co-expression of PNT1(1-31)-RFP and GFP-HELLP(214-271). An initial diffuse state
238 could however not be observed in this setting presumably as the result of the high
239 spontaneous conversion rate of the N-terminal GFP-HELLP(214-271) fusion (Table 1).

240 Finally, we tested the ability of the PNT1(1-31) to activate the HELLP effector protein. We
241 observed fusion cells between strains expressing PNT1(1-31) in the aggregated [π] state and
242 strains expressing full length HELLP (Fig 4C and 4D). We observed the localization of HELLP to
243 the plasma membrane region and cell death of the fusion cells. Thus, consistent with the
244 proposed role of HELLP as cell death execution protein activated by the PNT1 NLR, we find
245 that the PP-motif region of PNT1 forms a prion and is able to activate HELLP.

246

247 HET-S, HELLF and HELLP are components of three independent cell-death 248 inducing pathways

249 We previously reported a complete lack of cross-seeding between [Het-s] and [Φ] prions

250 despite identical backbone structures leading to the existence of two independent parallel
251 amyloid signaling pathways in *P. anserina* [20]. Here, we identified HELLP as an effector in a
252 third amyloid signaling pathway in *P. anserina*. To analyze HELLP/HELLF and HELLP/HET-s
253 interactions, we co-expressed HELLP(214-271) and HET-s or HELLF(209-271) respectively in a
254 *Δhellp Δhet-s Δhellf* strain. We observed the diffuse and foci states co-existing in all possible
255 combinations (Fig 5 and S4). Namely strains expressing HELLP(214-271) and HET-s could
256 display four different phenotypes : [Het-s]/[π] and [Het-s*]/[π∗] but also [Het-s]/[π∗] and [Het-
257 s*]/[π]. The same was true for HELLP(214-271) and HELLF(209-277 co-expression. These
258 results show that [Φ] or [Het-s] prions do not to convert [π*] and conversely that [π] prions
259 do not to convert [Φ*] or [Het-s*]. We also noted an absence of co-localization between
260 HELLP(214-271) and HET-s or HELLP(214-271) and HELLF(209-277) prion forms. Together,
261 these results demonstrated a lack of *in vivo* cross-seeding between the three *P. anserina* prion
262 forming domains.

263 We also monitored [π*] conversion by [Het-s] and [Φ] prions through barrage tests (S2
264 Table). Strains expressing HELLP(214-271)-GFP or -RFP and displaying [π*] phenotype were
265 confronted to strains expressing [π], [Φ] or [Het-s] prion forms and then tested for their ability
266 to form a barrage with tester strains expressing full length HELLP. Barrage were observed only
267 when the prion donor strain express [π] prions indicating that [π*] conversion do not occur in
268 presence of [Het-s] or [Φ] prions.

269 Finally, we analyzed the cross-activation of the cell death effectors of the three systems
270 by the different prions (S3 Table). Again, we used incompatibility assays and confronted [π],
271 [Φ] or [Het-s] prions expressing strains with strains expressing either HELLP, HELLF or HET-S
272 full-length proteins. We observed barrage formation solely when [π] strains were confronted
273 with HELLP expressing strains, [Φ] with HELLF and [Het-s] with HET-S, that is, when the prion

274 and the effector bear the same PFD. These results confirm that there is no cross-interaction
275 between these three amyloid signaling pathways.
276

277 *P. anserina* and *C. globosum* [π] prions cross-seed and co-localize

278 It was shown previously that HET-S PFDs homologs from *P. anserina* and *Fusarium*
279 *graminearum* which share about 38% identity do cross-seed [28]. We wondered whether the
280 45% similarity in the PFD region between HELLP and CgHELLP from *Chaetomium globosum*
281 would also allow for cross-seeding. To examine if the two PFD regions could co-aggregate *in*
282 *vivo*, strains co-expressing HELLP(214-271)-RFP and GFP-CgHELLP(215-278) were obtained
283 and analyzed by fluorescence microscopy (Fig 6A). As expected, we initially observed diffuse
284 fluorescence corresponding to the [π*] state and after a few days, foci appearing
285 concomitantly for the two proteins. There was no co-existence of soluble and aggregated
286 forms suggesting cross-conversion of HELLP and CgHELLP. Moreover, we observed a
287 significant co-localization indicating co-aggregation of the two prions *in vivo*. Upon
288 confrontation, [π] GFP-HELLP(214-271) donor converted GFP-CgHELLP(215-278) [π*] recipient
289 strains and conversely [π] CgHELLP(215-278) strains converted GFP-HELLP(214-271) [π*]
290 recipients (S4 Table).
291 We also used barrage assays to analyze the cross-induction of cell death activity of the
292 full-length CgHELLP and HELLP proteins (Fig 6B and S5 Table). GFP-CgHELLP(215-278) [π]
293 strains produced a barrage reaction to strain expressing HELLP and conversely GFP-HELLP(214-
294 271) [π] produced a barrage reaction to strain expressing CgHELLP. However, this was only
295 true when HELLP was highly expressed as a transgene. No barrage was observed in
296 confrontation to wild type. This result suggest that heterologous activation of HELLP by GFP-

297 CgHELLP(215-278) is less efficient than homotypic activation by GFP-HELLP(214-271). We
298 conclude that the "species-barrier" for prion seeding can be crossed for these PP-motifs but
299 that nevertheless homotypic interaction appear more efficient to activate the cell death
300 activity of the full-length protein.
301

302 **The RHIM regions of human RIP3 and RIP1 kinases form prions in *P. anserina***

303 The PP-motif as found in HELLP shows sequence homology to the mammalian RHIM amyloid
304 motif. We thus envisioned that akin to the PP-motif, mammalian RHIMs might behave as PFDs
305 when expressed in Podospora. We expressed the RIP3(444-469) and the RIP1(524-551)
306 regions fused to GFP or RFP in *Δhellp Δhet-s Δhellf* strains (Fig 7). Initially fluorescence was
307 diffuse and cytoplasmic and foci appeared spontaneously after few days of growth. The rate
308 of spontaneous transition to the aggregated state was monitored as previously for HELLP
309 (Table 1). For RIP3(444-469), the rates were comparable to the PP-motif with the highest rate
310 observed when GFP is in N-terminal position. For the RIP1 RHIM motif, the spontaneous rate
311 of foci formation was much lower especially for the two GFP fusions. However, this difference
312 relates only to spontaneous foci formation as the induced conversion through cytoplasmic
313 infection (with the corresponding foci form) is equally effective for the RIP1 and RIP3 motifs
314 (Fig 8). In addition, strains expressing RIP1(524-551) foci induced formation of RIP3(444-469)
315 foci and the converse was true. To test the ability of the [Rhim] prions observed in *P. anserina*
316 to interact, we co-expressed RIP1(524-551) and RIP3(444-469) fused to GFP or RFP in the same
317 strain (S5 Fig). Diffuse fluorescence was observed for several days during which these two
318 proteins were in the soluble [Rhim*] state. Then, foci formed concomitantly and co-localized
319 in the cell, often in the close vicinity of the septa where they appeared as aligned dots. The
320 concomitant emergence of RIP1 and RIP3 aggregates and their co-localization showed that

321 the [Rhim] prions co-aggregate and confirm RIP1(524-551) and RIP3(444-469) cross-seeding
322 *in vivo* in *P. anserina*.
323 We conclude that, the RHIM containing RIP3(444-469) and RIP1(524-551) regions behave
324 as PFDs *in vivo* in *P. anserina* and lead to the expression of two alternate phenotypes we
325 termed [Rhim*] and [Rhim]. In addition, the RIP1 and RIP3 [Rhim] prions cross-seed and co-
326 localize consistent with the fact that in mammalian cells and *in vitro*, RIP1 and RIP3 interact
327 through their RHIM regions to form amyloid heteropolymers [25].
328

329 **The [Rhim] and [π] prions partially cross-seed**

330 To examine possible interaction between [Rhim] and [π] prions, we analyzed the ability of the
331 prion containing strains to cross convert prion-free strains. For this purpose, strains expressing
332 HELLP(214-271)-RFP [π*], GFP-RIP3(444-496) and GFP-RIP1(524-551) [Rhim*] strains were
333 confronted with [π] and [Rhim] strains (Fig 8). After four days, the recipient strains were
334 sampled and subcultured and analyzed for the presence of foci by fluorescence microscopy.
335 In these conditions spontaneous prion formation was in the range of 10 to 20% for all
336 constructs. Homotypic interactions led to 80 to 90% prion conversion. High conversion rates
337 were observed for heterotypic conversion of GFP-RIP3(444-496) [Rhim*] by GFP-RIP1(524-
338 551) [Rhim]; and GFP-RIP1(524-551) [Rhim*] by GFP-RIP3(444-496) [Rhim]). Importantly, [π]
339 prions induced formation of both [Rhim] prions at a rate of about 60%. Conversely, both
340 [Rhim] prions induced formation of [π] prions at a similar rate (Fig 8). The results clearly
341 showed the ability of cross conversion between [Rhim] and [π] prions. The conversion is
342 however less efficient as in the case of homotypic interactions.
343 We also tested the ability of the two [Rhim] prions to induce the conversion of [Het-

344 s*] strains to the [Het-s] phenotype and observed a total absence of induction of this
345 conversion. This result is in line with the previous results concerning the absence of cross-
346 interaction between [π] and the other amyloid signaling pathways of *P. anserina* and rather
347 expected.

348 To explore interactions between [π] and [Rhim] further, HELLP and RIP1 (or RIP3) PFDs
349 fused to GFP or RFP were coexpressed in the same strain and transformants were analyzed by
350 fluorescence microscopy (Fig 9 and S6). Just after transfection, we observed diffuse signals for
351 both proteins (top panels in Fig 9A-B and S6A-B). It is possible to observe transformants where
352 one of the protein has already shifted towards the aggregated form while the other remained
353 soluble, with for instance, the coexistence of [π*] and [Rhim] phenotypes (Fig 9A and S6A) or
354 of [π] and [Rhim*] phenotypes (Fig 9B and S6B). In the combination RIP3(444-469)/HELLP(214-
355 271), most often spontaneous conversion to the [Rhim] phenotype is observed first,
356 consistent with the higher aggregation rate measured for RIP3(444-469) (Table 1). On the
357 contrary, in the RIP1(524-551)/HELLP(214-271) combination, the [π] prion appeared first,
358 again consistent with the measured lower spontaneous conversion rate of RIP1(524-551). In
359 both cases, upon further subculture, we observed foci for the two proteins that partially co-
360 localized (Fig 9A-B and S6A-B, bottom lines). Most often, the majority of the foci co-localized
361 while few others corresponded only to GFP or RFP-only foci. In addition, even in mixed foci
362 the co-localization is not absolute with RFP and GFP fluorescence that only partially
363 overlapped. Strains co-expressing RIP3(444-469) fused with GFP and RFP, or RIP1(524-551)
364 fused with GFP and RFP were used as positive control (S6C Fig) and showed co-localization
365 with almost perfectly overlapping foci. This phenomenon of patchy co-localization has already
366 been observed during coexpression of the HET-s proteins of *F. graminearum* and *P. anserina*
367 [28]. The same experiments were also carried out with CgHELLP(215-278) and the same results

368 were obtained (S7 Fig). These results indicate partial co-localization of [Rhim] and [π] prions,
369 a situation that is distinct both from the total lack of interaction seen between [π] and [Het-s]
370 and [Φ] prions and from the strong interactions seen between RIP1 and RIP3 [Rhim] prions on
371 one hand and HELLP and CgHELLP [π] prions on the other hand.
372

373 **[Rhim] prions induce toxicity of full length HELLP**

374 Confrontation of [Rhim] strains and full-length HELLP expressing strains did not lead to
375 barrage formation but microscopic observation of the confrontation zone revealed cell death
376 in few mixed cells (S8 Fig). We thus co-expressed in the same strain GFP-RIP3(444-469) or GFP-
377 RIP1(524-551) and HELLP-RFP to determine whether [Rhim] prions could induce HELLP
378 toxicity. Fluorescence signals were diffuse and cytoplasmic for both of the proteins and
379 remained stable for weeks indicating that [Rhim*] state remained much more stable in these
380 transformants than in GFP-RIP3(444-469) single transformants showing high rates of
381 spontaneous prion acquisition. To force transition to the [Rhim] state, these transformants
382 were confronted with [Rhim] strains and subsequently subcultured. After contact, about 60%
383 of the GFP-RIP3(444-469) [Rhim]/HELLP transformants displayed altered phenotypes with
384 reduced growth, 20% displayed sub-lethal phenotypes and only 20% showed normal growth.
385 Similarly in the case of GFP-RIP1(524-551) [Rhim]/HELLP coexpression 56% of the
386 transformants displayed altered phenotypes, 25% sub-lethal phenotypes and 19% appeared
387 normal. A representative sample of the abnormal transformants is shown (Fig 10A).
388 Fluorescence microscopy on these abnormal strains (Fig 10B) revealed not only the presence
389 of [Rhim] dots but also HELLP relocalization to the membrane associated with cell death,
390 swollen cells that were associated with sub-lethal growth, and HELLP aggregation in dots that

391 co-localized with [Rhim] dots in strains with altered growth phenotypes. On the contrary,
392 strains presenting normal growth rates either showed a [Rhim*] phenotype or showed an
393 important loss of fluorescence intensity for one or both of the co-expressed proteins. In the
394 same way, upon further sub-culturing transformants presenting growth defects often
395 "escaped" and presented normal growth associated with loss of fluorescence levels or of the
396 [Rhim] phenotype. These results suggest that [Rhim] prions are able to interact with HELLP
397 and to trigger trans-conformation of the full-length protein leading to cell membrane
398 relocalization and cell death. These results are in agreement with the partial [Rhim] and [π]
399 cross-seeding observed before. Similar results were obtained for CgHELLP, strains co-
400 expressing CgHELLP and GFP-RIP3(444-469) or GFP-RIP1(524-551) displayed altered growth
401 after contact with strains [Rhim] strains (S9 Fig).
402

403 # Discussion

404 A number of innate immune pathways function following a principle of "signaling by
405 cooperative assembly formation" (SCAF) [29]. Upon recognition of PAMPs or MAMPs,
406 receptors assemble into higher-order complexes or "supramolecular organizing centres"
407 (SMOCs) [30]. Following ligand recognition, the sensor modules oligomerize and recruit
408 adaptor or effector proteins -often via homotypic interactions- that further amplify the
409 oligomerization process and form cooperative, open-ended polymers (typically filaments).
410 This general scheme applies to many immune signaling modules including the RIG-I-like
411 receptors, the AIM2-like receptors and to NLRs. Formation of higher-order assemblies entitles
412 such signaling cascade with signal amplification, sharp threshold behavior and noise
413 reduction. In fact, this so-called prion-like polymerization process can involve nucleation of

414 either folded globular domains such as the TIR or Death domains [31,32] or short amyloid
415 motifs. The first such motif is RHIM identified in the necroptosis pathway in mammals and
416 allows for assembly of the necrosome formed by the RIP1 and RIP3 kinases [23]. RHIM-like
417 motif also regulate amyloid formation in innate immune cascades in Drosophila [24]. In
418 addition, several NLR-associated amyloid signaling motifs were identified in filamentous fungi
419 and more recently in multicellular bacteria [18,33]. Among them is the PP-motif that shows
420 similarity to the animal RHIM and RHIM-like motifs [22]. We identify here in the species
421 *Podospora anserina*, a PP-motif two-component system comprising a NLR termed PNT1 and a
422 cell-death execution protein termed HELLP. We showed that the HELLP PP-motif supports
423 prion propagation *in vivo* and leads to amyloid formation *in vitro*. We generated an artificial
424 incompatibility system based on HELLP, analogous to the natural [Het-s]/HET-S system, where
425 a truncated form of HELLP containing the PP motif is equivalent to [Het-s] and the full length
426 HELLP to HET-S. The N-terminal HELL domain of HELLP shows homology to the 4HB domain of
427 MLKL responsible for membrane permeation in mammalian necroptosis. HELLP induced
428 programmed cell death thus appears to be related to a family of evolutionary widespread form
429 of immune PCD which encompasses fungal cell death, necroptosis and cell death associated
430 with the hypersensitive response in plants [22,34,35]. We propose that PNT1 and HELLP
431 constitute a third amyloid immune-related signaling cascade controlling cell fate in *P.*
432 *anserina*. We show a total absence of cross-induction between the three *P. anserina* systems
433 allowing for the co-existence of three independent amyloid signaling cascades in the same
434 species. We find that in addition to the originally described NWD2/HET-S pathway, Podospora
435 possesses two additional PCD pathways. It is believed that fungal NLRs akin to their plant and
436 animal counterparts represent innate immune receptors that regulate response to pathogen
437 and symbiotic interactions in fungi. The three amyloid-associated NLRs identified in Podospora

438 share the fact that their WD or TPR repeat ligand binding domain is highly polymorphic in
439 natural populations consistent with the proposed role as immune receptor [13,14]. Yet, except
440 in the specific case of NLRs involved in incompatibility systems the nature of the ligands
441 activating these NLRs are currently unknown. Compared to the two other systems, the
442 NWD2/HET-S is characterized by the fact that this system has been exaptated as an
443 allorecognition system in [Het-s]/HET-S incompatibility [36]. It has been possible
444 experimentally, to derive incompatibility systems analogous to [Het-s]/HET-S from both HELLP
445 and HELLF. It will be of interest in the future to survey, natural Podospora strains to determine
446 whether exaptation of allorecognition incompatibility might have also occurred from HELLP
447 and HELLF. It is also of note, that the *Chaetomium globosum* and *Podospora anserina* PP-based
448 signalosome differ in the sense that the *Chaetomium* system has three components and
449 involves also CgSBP, a lipase also comprising a PP-motif and that is targeted to the membrane
450 region by CgHELLP. HELLP and CgHELLP should thus not be consider to be orthologs, as
451 supported by the fact that the two proteins share 39.6% identify while PNT1 and CgPNT1 show
452 only 25.2% identity.

453 So far, four mammalian proteins involved in necroptosis and five drosophila proteins also
454 involved in immune signaling have been described for RHIM-based amyloid signal
455 transduction [23,24]. The fact that a range of viruses express RHIM containing proteins and
456 that pathogenic bacteria express an enzyme that specifically cleave host RHIMs to prevent
457 necrosome assembly highlight the crucial role of RHIM-based interactions in the host innate
458 immune response against microbial infection [37]. As PP-motifs of Cg and HELLP resemble
459 RHIM motifs. This similarity is concentrate in the central G-X-Q-X-G core of the motif.
460 Mompeán and co-workers resolved the structure of human RIP1-RIP3 core as a serpentine
461 fold with turns and kinks resulting in an enclosed oblong-shaped hydrophobic core stabilized

462 by N and Q ladders and Y stacking [25]. RHIM-related motif appear to represents a new class
463 of amyloid fold distinct from the HRAM β-solenoid fold of HET-s but nonetheless presenting
464 common features with them as with other amyloid forming domains such as conservation of
465 G/N/Q residues. N and Q allow for formation of H-bonded N/Q ladders and G connect short
466 adjacent β-strands [11,38–40]. The fungal PP-motifs show strong conservation of the
467 pseudopalindromic structure centered on the Q residue along with conservation of flanking N
468 and G residues. We find here that the RHIM motifs of RIP1 and RIP3 behave as PFDs when
469 expressed in Podospora and thus behave analogously to PP-motifs in that respect.
470 Importantly, we find that [Rhim] and [π] prions cross-seed, albeit not as efficiently as RHIM
471 motifs or fungal PP-motifs. These results suggest both a structural similarity between RHIM
472 and PP-amyloids and substantial differences since the efficiency of prion seeding is clearly
473 distinct from that of homotypic or intraspecific seeding. Extensive structural analyses of the
474 amyloid fibers of HELLP or CgHELLP will be required to determine to which extend PP-based
475 amyloid polymers share the same fold as RIP1-RIP3. It appears however that the partial cross
476 seeding between PP and RHIM support a model of a common evolutionary origin of the two
477 motifs. In this context, it is interesting to note that in addition to the RHIM-like motifs
478 described in Drosophila a RHIM-related amyloid motif termed BASS3 was also identified in
479 multicellular bacteria [33]. It might be that the RHIM-related motif represent an archetypal
480 amyloid motif largely shared through evolution while other motifs such as HRAMs or other
481 bacterial signaling motifs have a more restricted phylogenetic distribution.
482

483 # Materials and Methods

484 ## Gene annotation

485 The Pa_5_8070 and Pa_5_8060 genes were annotated manually using two intron prediction
486 softwares, the GENSCAN Web server at MIT (genes.mit.edu/GENSCAN.html) and the
487 NetGene2 Web server (www.cbs.dtu.dk/services/NetGene2/), and using blastn searches
488 against EST sequences at ncbi and RNASEQ data from [41]. A single 47pb intron was identified
489 in nucleotide position 429 to 475 of the ORF of Pa_5_8070, this newly defined ORF encodes a
490 271 aa protein named HELLP. A single intron of 54 pb was identified in nucleotide position 95
491 to 148 of the ORF of Pa_5_8060, repeats number in the 3' part of the ORF is variable in *P.*
492 *anserina* strains, we described here the ORF of the S Orsay reference strain encoding a 971 aa
493 protein named PNT1.
494

495 **Strains and plasmids**

496 The *P. anserina* strains used in this study were wild-type *het-s* or *het-S* and the strains *Δhellp*
497 (*ΔPa_5_8070*) *het-s°* [22] and *Δhellp (ΔPa_5_8070) Δhet-s (ΔPa_3_620) Δhellf (ΔPa_3_9900)*
498 obtained by crossing the *Δhet-s Δhellf* strain [20] with the *Δhellp het-s°* strain. The *Δhellp het-s°*
499 strain was used as recipient strain for the expression of molecular fusions of full length HELLP
500 or PP motif-containing regions of HELLP and the GFP (green fluorescent protein) or RFP (red
501 fluorescent protein). These fusions were expressed from plasmids based on the pGEM-T
502 backbone (Promega) named pOP plasmids [22], containing either the GFP or RFP, or in a
503 derivative of the pAN52.1 GFP vector [27], named pGB6-GFP plasmid. In both cases, the
504 molecular fusions were under the control of the constitutive *P. anserina* gpd (glyceraldehyde-
505 3-phosphate dehydrogenase) promoter. The *Δhellp het-s°* strain was transformed as described
506 [42] with a fusion construct along with a second vector carrying a phleomycin-resistance gene
507 ble, pPaBle (using a 10:1 molar ratio). Phleomycin-resistant transformants were selected,
508 grown for 30 h at 26°C and screened for the expression of the transgenes using a fluorescence

509 microscope. The *hellp* gene and the *hellp(171-271)* and *hellp(214-271)* gene fragments were
510 amplified with the respective 5' forward oligonucleotides 5'
511 ggcttaattaaATGGATCCTCTCAGTATCACAGC 3', 5' ggcttaattaaATGATCACAGCGACAAACGATCAG
512 3' and 5' ggcttaattaaATGAAAGTACTGCATGAATCGCGC 3' and a same 3' reverse
513 oligonucleotide 5' ggcagatcttgctccCCCCCTTCGGCCAAATGTAG 3' (capital letters correspond to
514 *P. anserina* genomic DNA sequences). The PCR products were cloned upstream of the GFP or
515 RFP coding sequence in the pOP plasmids using PacI/BglII restriction enzymes to generate the
516 pOPhellp-GFP, pOPhellp-RFP, pOPhellp(171-271)-GFP, pOPhellp(171-271)-RFP, pOPhellp(214-
517 271)-GFP and pOPhellp(214-271)-RFP vectors in which in addition to the BglII site, a two aa
518 linker (GA) was introduced between the sequences encoding HELLP and GFP or RFP. *hellp(171-*
519 *271)* and *hellp(214-271)* were also amplified with the respective 5' forward oligonucleotides
520 5' ggcgcgcggccgcATCACAGCGACAAACGATCAG 3', 5'
521 ggcgcgcggccgcATCACAGCGACAAACGATCAG 3' and the same 3' reverse oligonucleotide 5'
522 ggcggatccCTACCCCCTTCGGCCAAATG 3' and cloned downstream of the GFP using NotI/BamHI
523 restriction enzymes to generate the plasmids pGB6-GFP-hellp(171-271) and pGB6-GFP-
524 hellp(214-271).

525 To investigate the co-localization/cross-seeding of HELLP with CgHELLP or of HELLP with
526 HELLF or HET-s, the *Δhellp Δhet-s Δhellf* strain was transformed both with vectors expressing
527 fluorescently tagged versions of full length or partial HELLP described above and with
528 fluorescently tagged versions of full length or partial HELLF, HET-s, HET-S or CgHELLP
529 previously described [20,22,27]: pOPhellf-GFP, pOPhellf(209-277)-RFP, pOPhellf(209-277)-
530 GFP, pOPhellf(L52K)-GFP, pOPhet-s-RFP, pGPD-het-S-GFP, pOPhet-S-RFP, pGB6-GFP-
531 Cghellp(215-278).

532 In the same way the sequence encoding the first 31 aa of *pnt1 (Pa_5_8060)* was amplified

533 with oligonucleotides 5' ggcttaattaaATGTCAGACAGTTATCGTTTCGGC 3' and 5'
534 ggcagatcttgctccTGGCGCCTGCAGGAAAGTATTG 3' and cloned in the pOP plasmids using
535 PacI/BglII restriction enzymes to generate the pOPpnt1(1-31)-GFP and the pOPpnt1(1-31)-
536 RFP. The *Δhellp Δhet-s Δhellf* strain was transformed with these vectors (and pPaBle) either
537 alone or with pOPhellp(214-271)-RFP or pGB6-GFP-hellp(214-271).

538 For heterologous expression in *E. coli*, we cloned *hellp(214-271)* in pET24 (Novagen) using
539 the NdeI/XhoI restrictions sites. The gene fragment *hellp(214-271)* was amplified with
540 oligonucleotides 5' agccatatgAAAGTACTGCATGAATCGCGC 3' and 5'
541 agcctcgagCCCCCTTCGGCCAAATGTAG 3' and cloned in front of a polyhistidine-tag to generate
542 pET24-hellp(214-271)-6xhis plasmid.

543 For the expression of RIP3(444-469) and RIP1(524-551), PCR products were amplified with
544 5' ggcttaattaaATGGTTACCGGTCGTCCGCTG 3' and 5'
545 ggcagatcttgctccCTGCATGGTCAGGTAGTTGTTG 3' or 5' ggcgcggccgcGTTACCGGTCGTCCGCTGG
546 3' and 5' ggcGGATCCTTACTGCATGGTCAGGTAGTTG 3' for RIP3 and with 5'
547 ggcttaattaaATGACTGACGAATCCATCAAATACACC 3' and 5'
548 ggcagatcttgctccGCCGCCGATTTCCATGTAGTT 3' or 5'
549 ggcgcggccgcACTGACGAATCCATCAAATACACC 3' and 5'
550 ggcGGATCCTTAGCCGCCGATTTCCATGTAGTT 3' for RIP1 and cloned as described above in the
551 pOP plasmids using PacI/BglII restriction enzymes, or in pGB6-GFP plasmid using NotI/BamHI
552 restriction enzymes.

553

554 **Prion propagation and incompatibility assays.**

555 Methods for determination of incompatibility phenotypes, prion formation and prion
556 propagation were as previously described [20,43]. In brief, incompatibility phenotypes were

557 determined by confronting strains on solid corn meal agar medium and a 'barrage' reaction
558 (abnormal contact lines forming upon confrontation of incompatible strains) was assessed 3
559 days post-contact. The [π] phenotype (acquisition of the [π] prion) was assessed as the ability
560 of a strain to form a barrage with a wild type strain or with a *Δhellp* bearing a transgene
561 encoding full length HELLP in fusion with GFP or RFP, named tester strain. [π] prion formation
562 can be measured as the rate of spontaneous acquired [π] prion phenotype in [π*] subculture
563 after 4 to 15 days of growth at 26°C on corn meal agar or as the ability to propagate [π] prion
564 form a donor strain to a [π*] prion-free strain. In the latter case, the donor strain can contain
565 the [π] prion (strains expressing HELLP or CgHELLP PFD) or another prion containing strain like
566 [Het-s] or [Φ] and is placed in contact for 3 days with the [π*] prion-free strain consecutively
567 tested in barrage assay with a tester strain. Cross reaction between the different prion systems
568 was also assessed in barrage tests as the ability of a prion containing strain (either [π], [Het-s]
569 or [Φ]) to form a barrage with a strain expressing one of the full length HeLo or HELL containing
570 proteins HELLP, CgHELLP, HELLF or HET-S. In these experiments strains previously described
571 by Daskalov and colleagues were used [20,22].
572

573 **Microscopy**

574 *P. anserina* hyphae were inoculated on solid medium and cultivated for 24 to 72 h at 26°C.
575 The medium was then cut out, placed on a glass slide and examined with a Leica DMRXA
576 microscope equipped with a Micromax CCD (Princeton Instruments) controlled by the
577 Metamorph 5.06 software (Roper Scientific). The microscope was fitted with a Leica PL APO
578 100X immersion lens. To observe cell death reaction and HELLP plasma membrane re-
579 localization, HELLP-GFP or HELLP-RFP expressing strains were inoculated at a distance of 2 cm

580 from a strain expressing one of the HELLP PFD containing fusion or the PNT1(1-31)-GFP or -
581 RFP. The confrontation zone between the two strains was observed hours after contact. For
582 Evans blue staining, an aqueous 0.001% solution was put directly on the mycelium for 5 min
583 followed by washing with distilled water before observation as described above.

584 For HELLP fibrils observations, negative staining was performed: aggregated proteins
585 were adsorbed onto Formvar-coated copper grids (400 mesh) and allowed to dry for 15 min
586 in air, grids were then negatively stained 1 min with 10 µL of freshly prepared 2% uranyl
587 acetate in water, dried with filter paper, and examined with a Hitachi H7650 transmission
588 electron microscope (Hitachi, Krefeld, Germany) at an accelerating voltage of 120 kV. TEM was
589 performed at the Pôle Imagerie Électronique of the Bordeaux Imaging Center using a Gatan
590 USC1000 2k x 2k camera.

591

592 **Protein preparation and fibril formation**

593 HELLP(214-271) protein was expressed in *E. coli* BL21-CodonPlus®-RP competent cells as
594 insoluble proteins and purified under denaturing conditions using its terminal 6 histidine tag
595 as previously described [44]. Briefly, cells were grown at 37°C in DYT medium to 0.6 OD_{600} and
596 expression was induced with 1 mM isopropyl β-D-1-thiogalactopyranoside. After, 4 h, cells
597 were harvested by centrifugation, frozen at -80°C sonicated on ice in a lysis buffer (Tris 50
598 mM, 150 mM NaCl, pH 8) and centrifuged for 20 min at 20,000 g to remove *E. coli*
599 contaminants. The pellet containing HELLP(214-271) in inclusion bodies was washed in the
600 same buffer and resuspended in denaturing buffer (8M guanidinium HCl, 150 mM NaCl, and
601 100 mM Tris-HCl, pH 8) until complete solubilization. The lysate was incubated with Talon
602 Resin (CLONTECH) for 1 h at 20°C, and the resin was extensively washed with 8 M urea, 150
603 mM NaCl, and 100 mM Tris-HCl, pH 8. The protein was eluted from the resin in the same buffer

604 containing 200 mM imidazole. The protein HELLP(214-271) was pure as judged by sodium-
605 dodecyl-sulfate polyacrylamide-gel electrophoreses (SDS-PAGE) followed by Coomassie-Blue
606 staining and yield was in the range of ~2-4 mg of protein per liter of culture. To eliminate urea,
607 elution buffer was replaced by overnight dialysis at 4°C against Milli-Q water. Fibrils formation
608 resulted spontaneously from dialysis process followed by sample storage at 4°C for 7 days.
609 Other conditions were used for sample preparation to test the influence of salt or acidic buffer
610 on the fibrils formation: presence or absence of 500 mM NaCl in the dialysis buffer,
611 replacement of dialysis by 50 times dilution in Milli-Q water or in ammonium acetate buffer
612 100 mM pH 4.5, they all resulted in spontaneous appearance of fibrils.
613

614 **Bioinformatic methods**

615 Blast analyses on the *P. anserina* genome were achieved on the *Podospora anserina* Genome
616 Project site (podospora.i2bc.paris-saclay.fr/). Sequence alignments were performed with
617 Clustal Omega or MAFFT at (www.ebi.ac.uk) and edited with Jalview (www.jalview.org/). To
618 generate the HMM profile signatures for PP and RHIM, psi-blast searches were performed at
619 (blast.ncbi.nlm.nih.gov) using the HELLP PP sequence and the RHIM motif of human RIP3 and
620 matching sequences were aligned with Clustal Omega and the alignment was analyzed with
621 Skylign (skylign.org). Secondary structure predictions were performed with PSIPRED
622 (bioinf.cs.ucl.ac.uk/psipred/). Hidden Markov Model searches were performed using HHPred
623 (toolkit.tuebingen.mpg.de) and Jackhhmer (www.ebi.ac.uk/Tools/hmmer/search/phmmer),
624 both with default settings. The prediction of transmembrane helix was performed with the
625 TMHMM server (www.cbs.dtu.dk/services/TMHMM).
626

Author Contributions

Conceptualization: Thierry Bardin, Asen Daskalov, Sven J. Saupe, Virginie Coustou

Data curation: Thierry Bardin, Asen Daskalov, Sophie Barrouilhet, Sven J. Saupe, Virginie Coustou

Formal analysis: Thierry Bardin, Asen Daskalov, Sophie Barrouilhet, Sven J. Saupe, Virginie Coustou

Funding acquisition: Sven J. Saupe

Investigation: Thierry Bardin, Asen Daskalov, Sophie Barrouilhet, Alexandra Granger-Farbos, Bénédicte Salin, Corinne Blancard, Virginie Coustou

Methodology: Thierry Bardin, Asen Daskalov, Alexandra Granger-Farbos, Bénédicte Salin, Corinne Blancard, Sven J. Saupe, Virginie Coustou

Project administration: Sven J. Saupe, Virginie Coustou

Resources: Alexandra Granger-Farbos, Bénédicte Salin, Corinne Blancard, Sven J. Saupe, Virginie Coustou

Supervision: Sven J. Saupe, Virginie Coustou

Validation: Thierry Bardin, Asen Daskalov, Sven J. Saupe, Virginie Coustou

Visualization: Thierry Bardin, Asen Daskalov, Sven J. Saupe, Virginie Coustou

Writing: Sven J. Saupe, Virginie Coustou

646 # References

647 1. Prusiner S. Novel proteinaceous infectious particles cause scrapie. Science. 1982;216: 136.
648 doi:10.1126/science.6801762

649 2. Colby DW, Prusiner SB. Prions. Cold Spring Harbor Perspectives in Biology. 2011;3: a006833–
650 a006833. doi:10.1101/cshperspect.a006833

651 3. Wickner RB, Edskes HK, Son M, Bezsonov EE, DeWilde M, Ducatez M. Yeast Prions Compared to
652 Functional Prions and Amyloids. Journal of Molecular Biology. 2018;430: 3707–3719.
653 doi:10.1016/j.jmb.2018.04.022

654 4. Coustou V, Deleu C, Saupe S, Begueret J. The protein product of the het-s heterokaryon
655 incompatibility gene of the fungus Podospora anserina behaves as a prion analog. Proc Natl Acad
656 Sci U S A. 1997;94: 9773–9778.

657 5. Saupe SJ. The [Het-s] prion of Podospora anserina and its role in heterokaryon incompatibility.
658 Semin Cell Dev Biol. 2011;22: 460–468. doi:10.1016/j.semcdb.2011.02.019

659 6. Balguerie A, Dos Reis S, Ritter C, Chaignepain S, Coulary-Salin B, Forge V, et al. Domain
660 organization and structure-function relationship of the HET-s prion protein of Podospora
661 anserina. EMBO J. 2003;22: 2071–2081. doi:10.1093/emboj/cdg213

662 7. Seuring C, Greenwald J, Wasmer C, Wepf R, Saupe SJ, Meier BH, et al. The mechanism of toxicity
663 in HET-S/HET-s prion incompatibility. PLoS Biol. 2012;10: e1001451.
664 doi:10.1371/journal.pbio.1001451

665 8. Nazabal A, Dos Reis S, Bonneu M, Saupe SJ, Schmitter J-M. Conformational transition occurring
666 upon amyloid aggregation of the HET-s prion protein of Podospora anserina analyzed by
667 hydrogen/deuterium exchange and mass spectrometry. Biochemistry. 2003;42: 8852–8861.
668 doi:10.1021/bi0344275

669 9. Ritter C, Maddelein M-L, Siemer AB, Lührs T, Ernst M, Meier BH, et al. Correlation of structural
670 elements and infectivity of the HET-s prion. Nature. 2005;435: 844–848.
671 doi:10.1038/nature03793

672 10. Sen A, Baxa U, Simon MN, Wall JS, Sabate R, Saupe SJ, et al. Mass analysis by scanning
673 transmission electron microscopy and electron diffraction validate predictions of stacked beta-
674 solenoid model of HET-s prion fibrils. J Biol Chem. 2007;282: 5545–5550.
675 doi:10.1074/jbc.M611464200

676 11. Wasmer C, Lange A, Van Melckebeke H, Siemer AB, Riek R, Meier BH. Amyloid fibrils of the HET-
677 s(218-289) prion form a beta solenoid with a triangular hydrophobic core. Science. 2008;319:
678 1523–1526. doi:10.1126/science.1151839

679 12. Mathur V, Seuring C, Riek R, Saupe SJ, Liebman SW. Localization of HET-S to the cell periphery,
680 not to [Het-s] aggregates, is associated with [Het-s]-HET-S toxicity. Mol Cell Biol. 2012;32: 139–
681 153. doi:10.1128/MCB.06125-11

682 13. Daskalov A, Habenstein B, Martinez D, Debets AJM, Sabaté R, Loquet A, et al. Signal transduction
683 by a fungal NOD-like receptor based on propagation of a prion amyloid fold. PLoS Biol. 2015;13:
684 e1002059. doi:10.1371/journal.pbio.1002059

685 14. Dyrka W, Lamacchia M, Durrens P, Kobe B, Daskalov A, Paoletti M, et al. Diversity and variability
686 of NOD-like receptors in fungi. Genome Biol Evol. 2014;6: 3137–3158. doi:10.1093/gbe/evu251

687 15. Jones JDG, Vance RE, Dangl JL. Intracellular innate immune surveillance devices in plants and
688 animals. Science. 2016;354. doi:10.1126/science.aaf6395

689 16. Daskalov A, Paoletti M, Ness F, Saupe SJ. Genomic clustering and homology between HET-S and
690 the NWD2 STAND protein in various fungal genomes. PLoS ONE. 2012;7: e34854.
691 doi:10.1371/journal.pone.0034854

692 17. Cai X, Chen J, Xu H, Liu S, Jiang Q-X, Halfmann R, et al. Prion-like polymerization underlies signal
693 transduction in antiviral immune defense and inflammasome activation. Cell. 2014;156: 1207–
694 1222. doi:10.1016/j.cell.2014.01.063

695 18. Loquet A, Saupe SJ. Diversity of Amyloid Motifs in NLR Signaling in Fungi. Biomolecules. 2017;7.
696 doi:10.3390/biom7020038

697 19. Daskalov A, Dyrka W, Saupe SJ. Theme and variations: evolutionary diversification of the HET-s
698 functional amyloid motif. Sci Rep. 2015;5: 12494. doi:10.1038/srep12494

699 20. Daskalov A, Martinez D, Coustou V, El Mammeri N, Berbon M, Andreas LB, et al. Structural and
700 molecular basis of cross-seeding barriers in amyloids. bioRxiv. 2020; 2020.07.06.188508.
701 Available from: https://www.biorxiv.org/content/10.1101/2020.07.06.188508v1.
702 doi:10.1101/2020.07.06.188508

703 21. Murphy JM, Czabotar PE, Hildebrand JM, Lucet IS, Zhang J-G, Alvarez-Diaz S, et al. The
704 Pseudokinase MLKL Mediates Necroptosis via a Molecular Switch Mechanism. Immunity.
705 2013;39: 443–453. doi:10.1016/j.immuni.2013.06.018

706 22. Daskalov A, Habenstein B, Sabaté R, Berbon M, Martinez D, Chaignepain S, et al. Identification of
707 a novel cell death-inducing domain reveals that fungal amyloid-controlled programmed cell
708 death is related to necroptosis. Proc Natl Acad Sci USA. 2016;113: 2720–2725.
709 doi:10.1073/pnas.1522361113

710 23. Li J, McQuade T, Siemer AB, Napetschnig J, Moriwaki K, Hsiao Y-S, et al. The RIP1/RIP3 Necrosome
711 Forms a Functional Amyloid Signaling Complex Required for Programmed Necrosis. Cell.
712 2012;150: 339–350. doi:10.1016/j.cell.2012.06.019

713 24. Kleino A, Ramia NF, Bozkurt G, Shen Y, Nailwal H, Huang J, et al. Peptidoglycan-Sensing Receptors
714 Trigger the Formation of Functional Amyloids of the Adaptor Protein Imd to Initiate Drosophila
715 NF-κB Signaling. Immunity. 2017;47: 635-647.e6. doi:10.1016/j.immuni.2017.09.011

716 25. Mompeán M, Li W, Li J, Laage S, Siemer AB, Bozkurt G, et al. The Structure of the Necrosome
717 RIPK1-RIPK3 Core, a Human Hetero-Amyloid Signaling Complex. Cell. 2018;173: 1244-1253.e10.
718 doi:10.1016/j.cell.2018.03.032

719 26. Beisson-Schecroun J. [Cellular incompatibility and nucleo-cytoplasmic interactions in the
720 “barrage” phenomena in Podospora anserina]. Ann Genet. 1962;4: 4–50.

721 27. Balguerie A, Dos Reis S, Coulary-Salin B, Chaignepain S, Sabourin M, Schmitter J-M, et al. The
722 sequences appended to the amyloid core region of the HET-s prion protein determine higher-
723 order aggregate organization in vivo. J Cell Sci. 2004;117: 2599–2610. doi:10.1242/jcs.01116

724 28. Benkemoun L, Ness F, Sabaté R, Ceschin J, Breton A, Clavé C, et al. Two structurally similar fungal
725 prions efficiently cross-seed in vivo but form distinct polymers when coexpressed. Mol Microbiol.
726 2011;82: 1392–1405. doi:10.1111/j.1365-2958.2011.07893.x

727 29. Nanson JD, Kobe B, Ve T. Death, TIR, and RHIM: Self-assembling domains involved in innate
728 immunity and cell-death signaling. J Leukoc Biol. 2019;105: 363–375. doi:10.1002/JLB.MR0318-
729 123R

730 30. Kagan JC, Magupalli VG, Wu H. SMOCs: supramolecular organizing centres that control innate
731 immunity. Nat Rev Immunol. 2014;14: 821–826. doi:10.1038/nri3757

732 31. Wu H. Higher-order assemblies in a new paradigm of signal transduction. Cell. 2013;153: 287–
733 292. doi:10.1016/j.cell.2013.03.013

734 32. Cai X, Chen ZJ. Prion-like polymerization as a signaling mechanism. Trends Immunol. 2014;35:
735 622–630. doi:10.1016/j.it.2014.10.003

736 33. Dyrka W, Coustou V, Daskalov A, Lends A, Bardin T, Berbon M, et al. Identification of NLR-
737 associated amyloid signaling motifs in filamentous bacteria. bioRxiv; 2020 Jan. Available from:
738 https://www.biorxiv.org/content/10.1101/2020.01.06.895854v1.
739 doi:10.1101/2020.01.06.895854

740 34. Burdett H, Bentham AR, Williams SJ, Dodds PN, Anderson PA, Banfield MJ, et al. The Plant
741 "Resistosome": Structural Insights into Immune Signaling. Cell Host & Microbe. 2019;26: 193–
742 201. doi:10.1016/j.chom.2019.07.020

743 35. Hofmann K. The Evolutionary Origins of Programmed Cell Death Signaling. Cold Spring Harb
744 Perspect Biol. 2019; a036442. doi:10.1101/cshperspect.a036442

745 36. Daskalov A, Saupe SJ. As a toxin dies a prion comes to life: A tentative natural history of the [Het-
746 s] prion. Prion. 2015;9: 184–189. doi:10.1080/19336896.2015.1038018

747 37. Baker MODG, Shanmugam N, Pham CLL, Strange M, Steain M, Sunde M. RHIM-based
748 protein:protein interactions in microbial defence against programmed cell death by necroptosis.
749 Seminars in Cell & Developmental Biology. 2018 [cited 11 Sep 2018].
750 doi:10.1016/j.semcdb.2018.05.004

751 38. Plumley JA, Dannenberg JJ. The importance of hydrogen bonding between the glutamine side
752 chains to the formation of amyloid VQIVYK parallel beta-sheets: an ONIOM DFT/AM1 study. J Am
753 Chem Soc. 2010;132: 1758–1759. doi:10.1021/ja909690a

754 39. Halfmann R, Alberti S, Krishnan R, Lyle N, O'Donnell CW, King OD, et al. Opposing effects of
755 glutamine and asparagine govern prion formation by intrinsically disordered proteins. Mol Cell.
756 2011;43: 72–84. doi:10.1016/j.molcel.2011.05.013

757 40. Tuttle MD, Comellas G, Nieuwkoop AJ, Covell DJ, Berthold DA, Kloepper KD, et al. Solid-state NMR
758 structure of a pathogenic fibril of full-length human α-synuclein. Nat Struct Mol Biol. 2016;23:
759 409–415. doi:10.1038/nsmb.3194

760 41. Lamacchia M, Dyrka W, Breton A, Saupe SJ, Paoletti M. Overlapping Podospora anserina
761 Transcriptional Responses to Bacterial and Fungal Non Self Indicate a Multilayered Innate
762 Immune Response. Front Microbiol. 2016;7: 471. doi:10.3389/fmicb.2016.00471

763 42. Bergès T, Barreau C. Heat shock at an elevated temperature improves transformation efficiency
764 of protoplasts from Podospora anserina. J Gen Microbiol. 1989;135: 601–604.
765 doi:10.1099/00221287-135-3-601

766 43. Benkemoun L, Sabaté R, Malato L, Dos Reis S, Dalstra H, Saupe SJ, et al. Methods for the in vivo
767 and in vitro analysis of [Het-s] prion infectivity. Methods. 2006;39: 61–67.
768 doi:10.1016/j.ymeth.2006.04.006

769 44. Dos Reis S, Coulary-Salin B, Forge V, Lascu I, Bégueret J, Saupe SJ. The HET-s prion protein of the
770 filamentous fungus Podospora anserina aggregates in vitro into amyloid-like fibrils. J Biol Chem.
771 2002;277: 5703–5706. doi:10.1074/jbc.M110183200

772

773 **FIGURES**

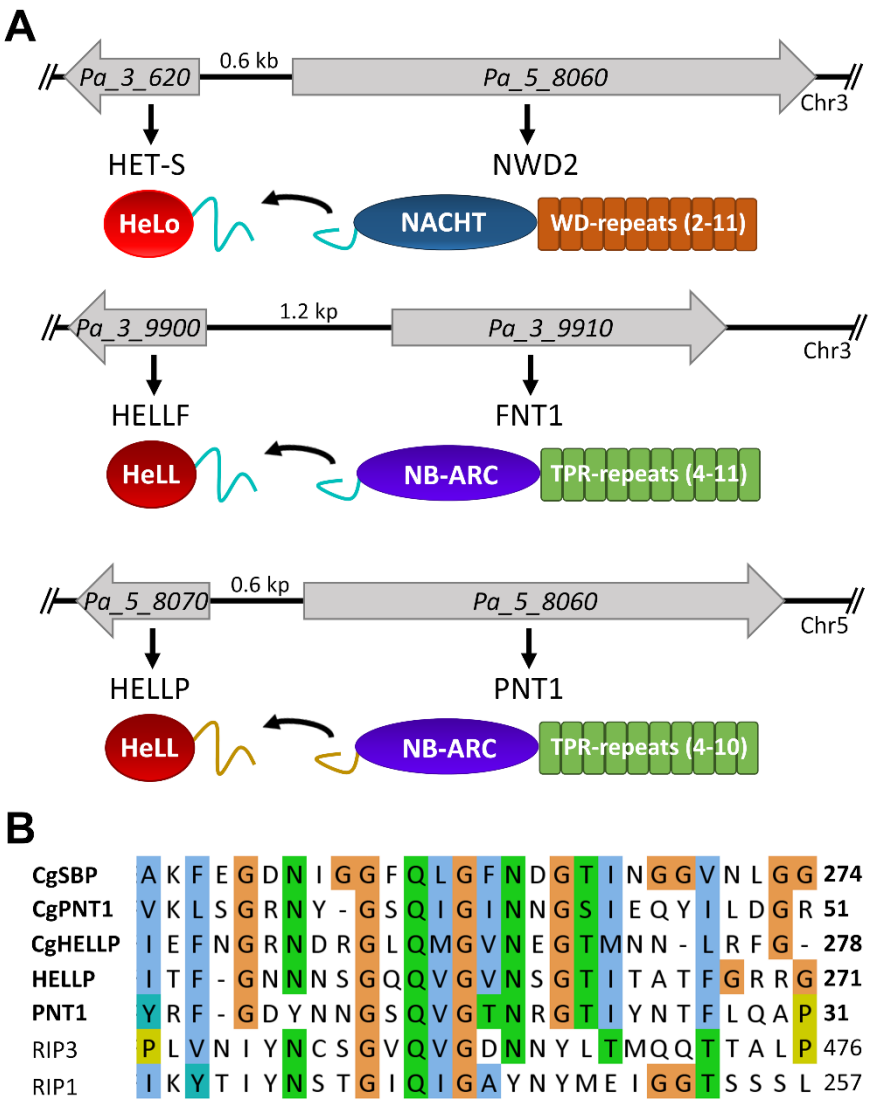

774

775 **Fig 1. The PP motif and the two HRAM motif gene clusters of *P. anserina.***

776 (A) Genome organization and domain architecture of the *het-s/nwd2*, *hellf/fnt1* and
777 *hellp/pnt1* gene clusters of *P. anserina*. These loci are composed of two adjacent genes
778 encoding an effector protein and a NLR receptor. The effector proteins are composed of a PFD
779 and a HeLo or HELL domain. The NLRs are composed of a PFD, a NB-ARC or NACHT nucleotide
780 binding domain and of WD or TPR repeats (repetition numbers is variable as indicated). PFDs
781 of the HRAM family are represented as a turquoise line while those of the PP family as a light-

782 brown line. (B) Alignment of the PP motifs of HELLP, PNT1, CgHELLP, CgSBP, and CgPNT1 along

783 with the RHIM motif of human RIP1 and RIP3.

784

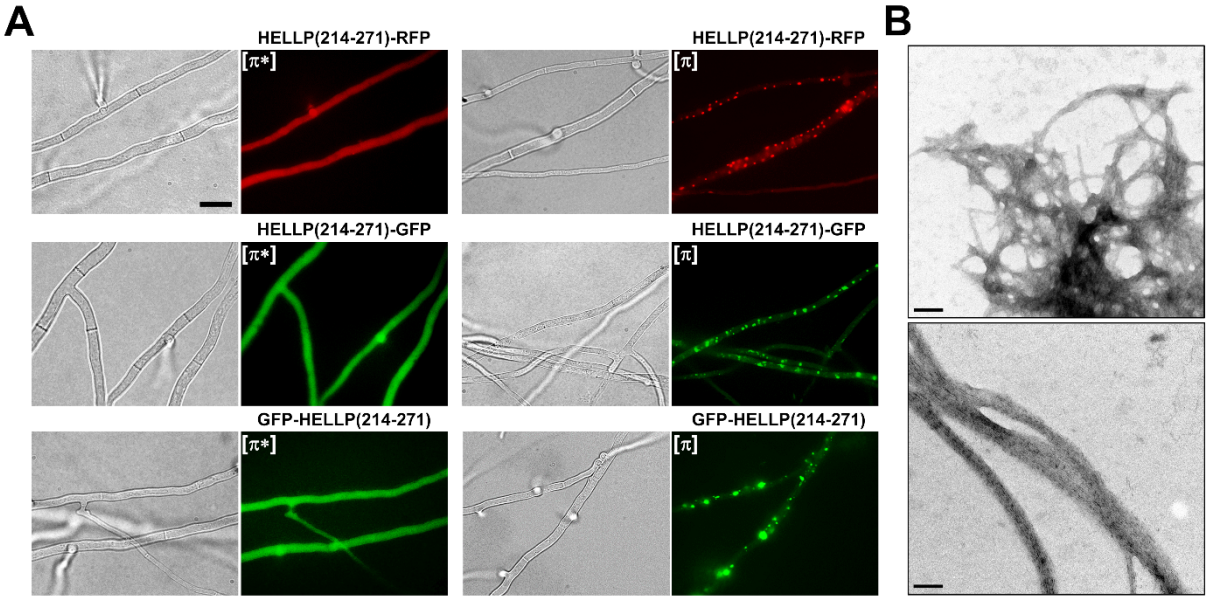

Fig 2. HELLP PP region behaves as a prion *in vivo* and forms fibrils *in vitro*

(A) Micrographs of *P. anserina* strains expressing different molecular fusions (HELLP(214-271-RFP/GFP, GFP-HELLP(214-271)) as indicated above each micrograph (Scale bar: 5 µm). Transformants present initially a diffuse fluorescence in the non-prion state designated [π*] (left) and acquire dot-like fluorescent aggregates after contact with a strain already expressing the infectious prion state designated [π] (right). (B) Electron micrograph of negatively stained HELLP(214-271) fibrils, scale bar is 100 nm.

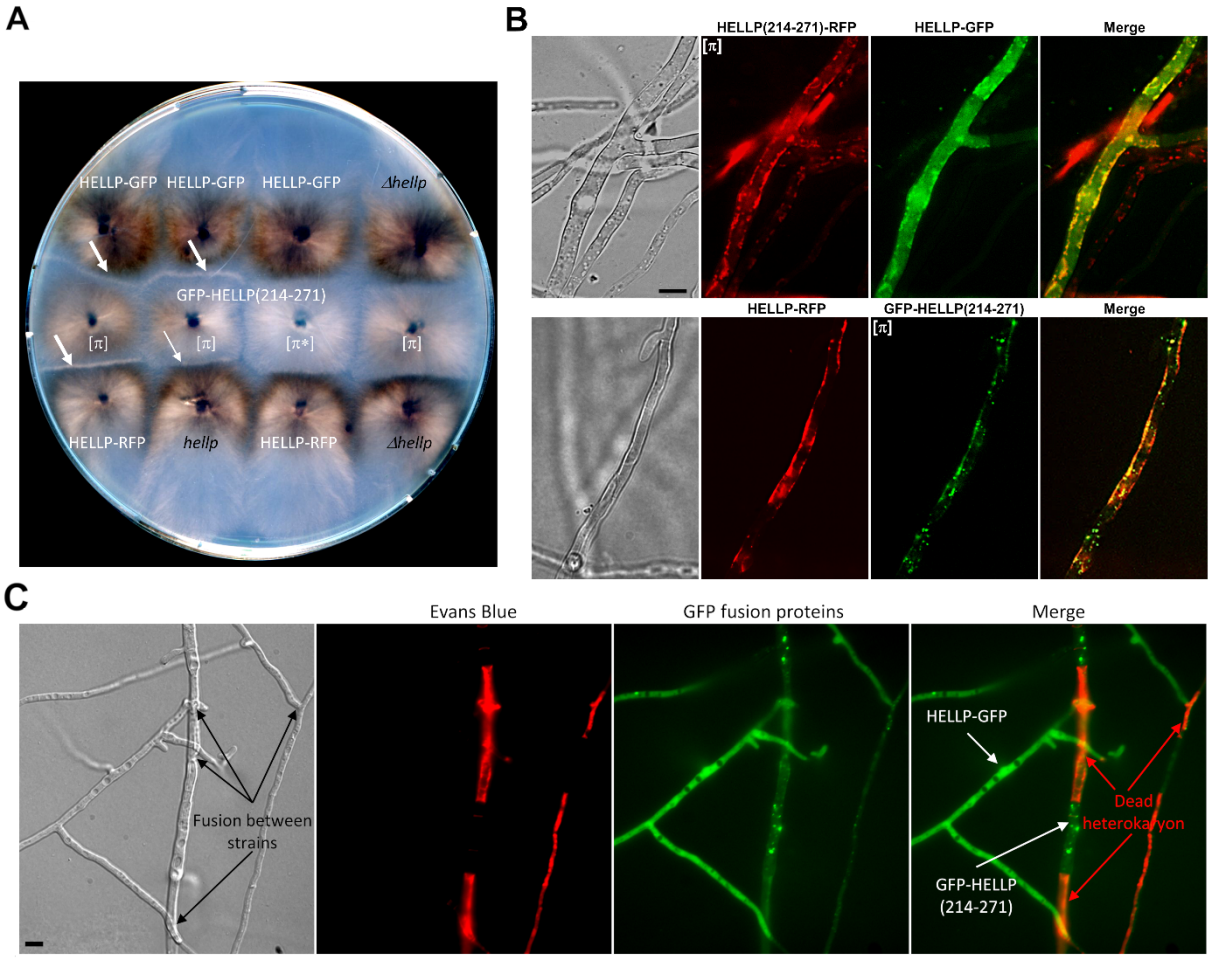

794

795 **Fig 3. Activation of HELLP cell death activity by [π] prion.**

796 (A) Observation of incompatibility reaction between [π] prion and HELLP in barrage tests.
797 Confrontation on solid medium of transformants expressing GFP-HELLP(214-271) in soluble
798 [π*] or aggregated [π] states with strains expressing full length HELLP from a transgene
799 (written in white) or from the wild type *hellp* gene or with the *Δhellp* strain as a negative
800 control. Formation of a barrage indicative of an incompatibility reaction is marked by a white
801 arrow. The thinner arrow indicates an attenuated barrage reaction. (B) Micrographs of fusion
802 cells coexpressing full-length HELLP (HELLP-GFP (upper panel) or HELLP-RFP (lower panel)),
803 and HELLP(214-271)-RFP (upper panel) or GFP-HELLP(214-271) (lower panel) in the [π]
804 aggregated state. Note that HELLP relocalizes to the cell membrane region in presence of [π].
805 (C) Micrographs showing confrontations between HELLP-GFP and GFP-HELLP(214-271)

806 expressing strains after Evans blue staining. Note that heterocaryotic fusion cells are stained

807 indicating their death. Scale bar (2 μm).

808

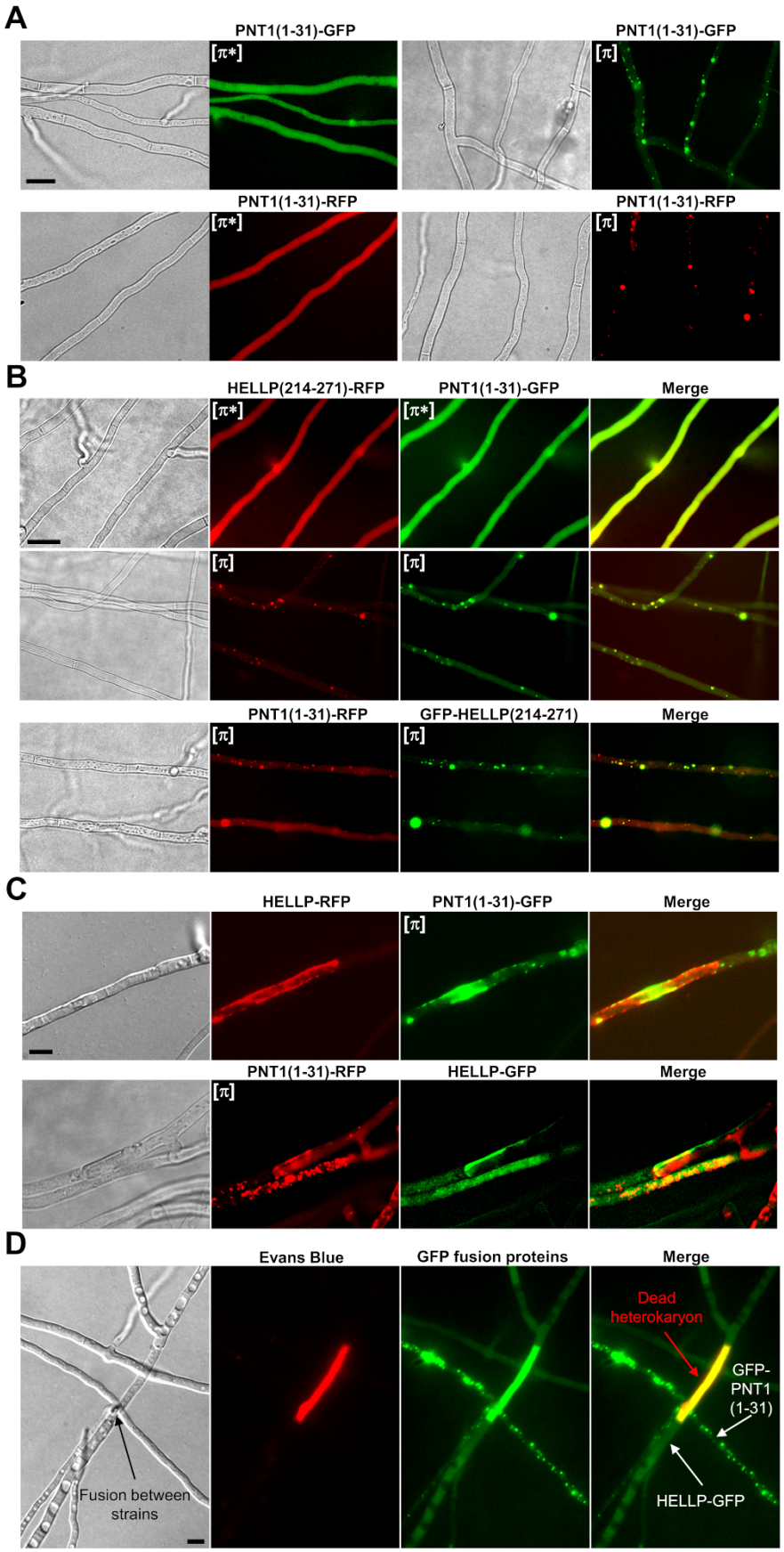
A
PNT1(1-31)-GFP
[π*]
PNT1(1-31)-GFP
[π]
PNT1(1-31)-RFP
[π*]
PNT1(1-31)-RFP
[π]
B
HELLP(214-271)-RFP
PNT1(1-31)-GFP
Merge
[π*]
[π*]
[π]
[π]
PNT1(1-31)-RFP
GFP-HELLP(214-271)
Merge
[π]
[π]
C
HELLP-RFP
PNT1(1-31)-GFP
Merge
[π]
PNT1(1-31)-RFP
HELLP-GFP
Merge
[π]
D
Evans Blue
GFP fusion proteins
Merge
Dead heterokaryon
GFP-PNT1 (1-31)
HELLP-GFP
Fusion between strains

809

810

811

812 **Fig 4. PNT1(1-31) aggregates *in vivo*, co-localizes with HELLP(214-271) and targets HELLP to**

813 **the plasma membrane.**

814 (A) Micrographs of PNT1(1-31) fusions with GFP or RFP either in the soluble state (left) or

815 aggregated state (right). (B) Micrographs showing co-localization of PNT1(1-31) and

816 HELLP(214-271) in soluble (top picture) or aggregated states. (C) In fusion cells coexpressing

817 full-length HELLP (fused with RFP (upper panel) or GFP (lower panel)), and aggregated forms

818 of PaPNT1(1-31) (fused with GFP (lower panel), or RFP, lower panel), HELLP relocalized to the

819 plasma membrane. Scale bar (2 μm). (D) Micrographs showing confrontations between HELLP-

820 GFP and GFP-PNT1(1-31) expressing strains after Evans blue staining. Note that heterocaryotic

821 fusion cells are stained indicating their death. Scale bar (2 μm).

822

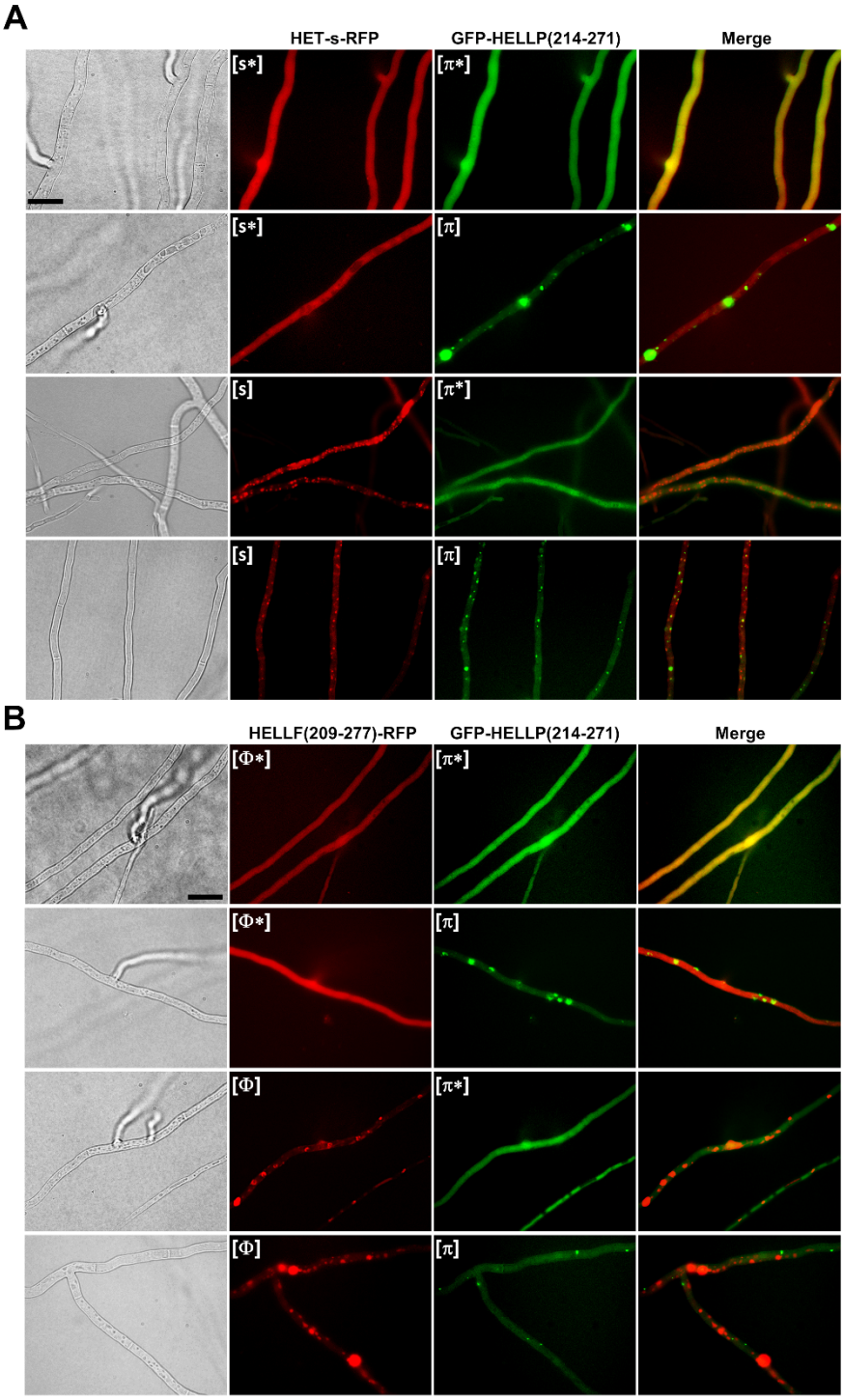

823

824 **Fig 5. Lack of cross-seeding *in vivo* between [π] and [Het-s] or [Φ] prions.**

825 (A) Micrographs of strains co-expressing HET-s-RFP ([Het-s] or [Het-s*] state) and GFP-

826 HELLP(214-271) ([π*] or [π] state). Note an absence of co-localization of the two aggregated

827 prion forms and the absence of conversion of [Het-s*] state by [π] prion and of [π*] by [Het-

828 s] prion. Scale bar (5 μm). (B) Micrographs of strains co-expressing HELLF(209-277)-RFP ([Φ]

829 or [Φ*] state) and GFP-HELLP(214-271) ([π*] or [π] state). Note an absence of co-localization

830 of the two aggregated prion forms and the absence of conversion of [Φ *] state by [π] prion

831 and of [π*] by [Φ] prion. Scale bar (5 μm).

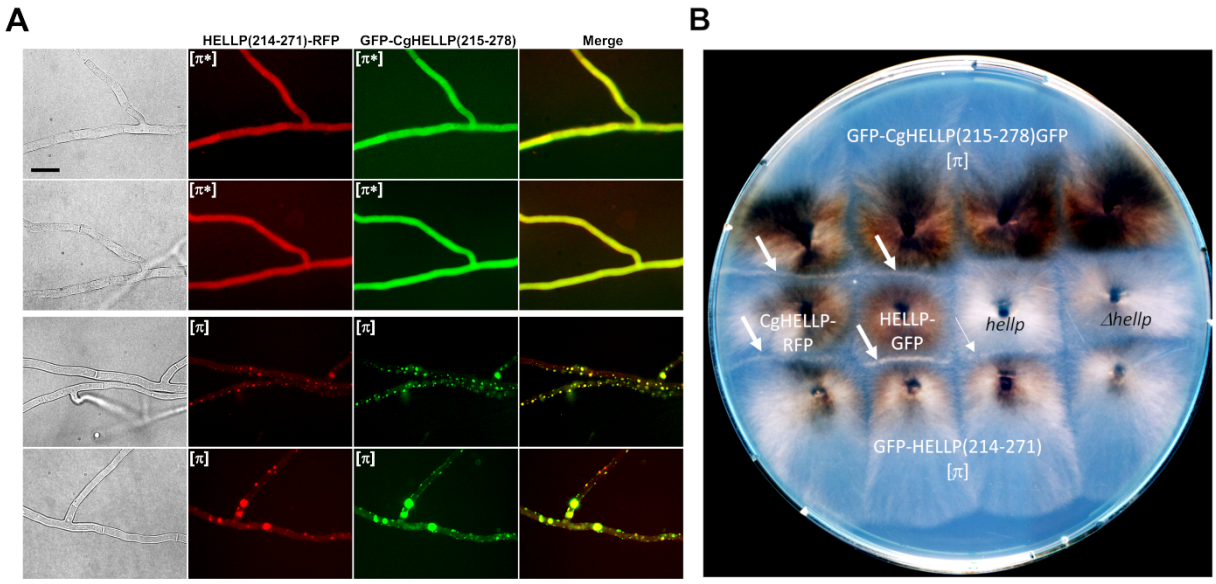

Fig 6. Co-localization of HELLP and CgHELLP PFDs and cross induction of cell death activity. (A) Micrographs of strains co-expressing HELLP(214-271)-RFP and GFP-CgHELLP(215-278) in soluble [π*] state (upper panels) or aggregated [π] state (lower panels). Note the co-localization of the two aggregated prion forms. Scale bar (5 μm). (B) Confrontation on solid medium of strains expressing GFP-HELLP(214-271) and GFP-CgHELLP(215-278) [π] prions forms with strains expressing full length HELLP from a transgene (written in white) or from the wild type *hellp* gene or with the *Δhellp* strain as a negative control. Formation of a barrage indicative of an incompatibility reaction is marked by a white arrow. The thinner arrow indicates an attenuated barrage reaction.

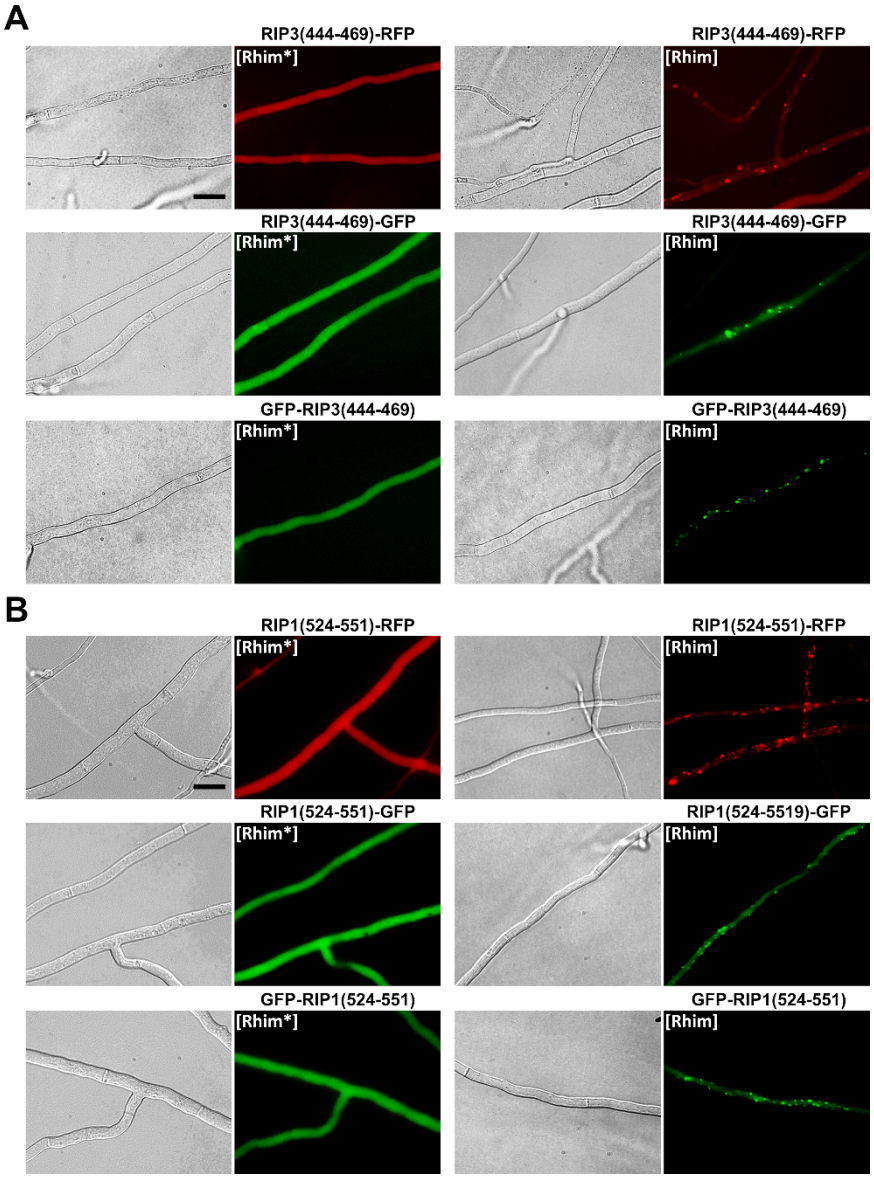

Fig 7. *In vivo* prion propagation of the human RIP3 and RIP1 RHIM regions.

(A) Micrographs of *P. anserina* strains expressing the molecular fusions RIP3(444-469)-RFP, RIP3(444-469)-GFP or GFP-RIP3(444-469). (B) Micrographs of *P. anserina* strains expressing the molecular fusions RIP1(524-551)-RFP, RIP1(524-551)-GFP or GFP-RIP1(524-551). (A and B) Transformants present initially a diffuse fluorescence in the non-prion state designated [Rhim*] (left) and acquire dot-like fluorescent aggregates after contact with a strain already expressing the infectious prion state designated [Rhim] (right). (Scale bar: 5 µm).

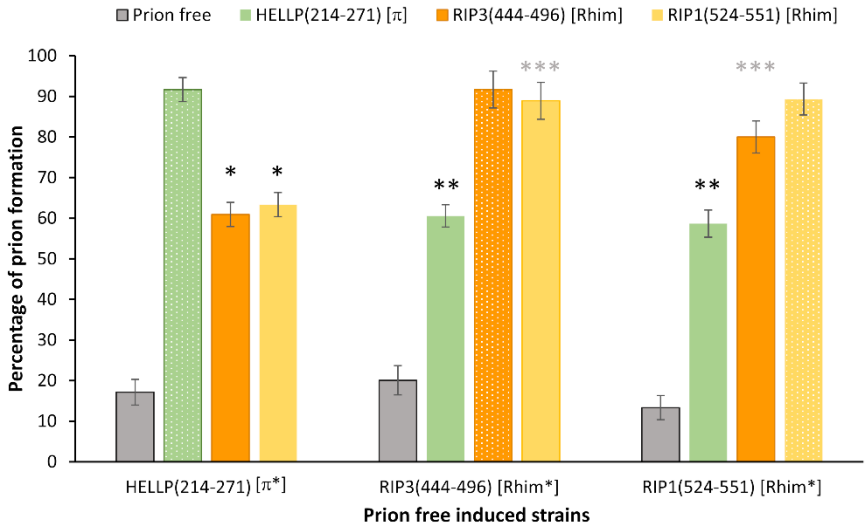

852

853 **Fig 8. Cross conversion between [π] and [Rhim] prions.**

854 Histograms representing the percentage of [π] and [Rhim] prion containing strains obtained
855 after contact of induced strains (initially displaying [π*] or [Rhim*] phenotype) with a
856 *Δhellp Δhet-s Δhellf* prion free strain (control), a GFP-HELLP(214-271) [π] containing strain or
857 GFP-RIP3(444-469) or GFP-RIP1(524-551) [Rhim] containing strains (indicated on top).
858 Phenotype after induction was determined by monitoring the acquisition of dot-like
859 aggregates by fluorescence microscopy as an indicator of the prion propagation. Percentages
860 of prion formation were expressed as the mean value ± standard deviation for 3 to 5
861 independent experiments on 4 different transformants. P-values for cross conversion were
862 determined using two tails Fisher's test by comparison of the number of prion free and prion
863 containing strains obtained after induction by the prion free control or by the heterotypic
864 prion containing strain.

865 *: p-values for cross conversion of HELLP(214-271) [π*] strains to [π] strains by GFP-RIP3(444-
866 496) [Rhim] or by GFP-RIP1(524-551) [Rhim] inducers were respectively $8.5x10^{-8}$ and $1.6x10^{-8}$.

867 **: p-values for cross conversion of GFP-RIP3(444-496) [Rhim*] or GFP-RIP1(524-551) [Rhim*]
868 strains to [Rhim] strains by HELLP(214-271) [π] inducer were respectively $3.8x10^{-8}$ and $7.2x10^{-}$

869 [8].

870 ***: p-values for cross conversion of GFP-RIP3(444-496) [Rhim*] to [Rhim] strains by GFP-

871 RIP1(524-551) [Rhim] inducer or GFP-RIP1(524-551) [Rhim*] to [Rhim] strains by GFP-

872 RIP3(444-496) [Rhim] inducer were respectively $1.5x10^{-16}$ and $3.2x10^{-16}$.

873

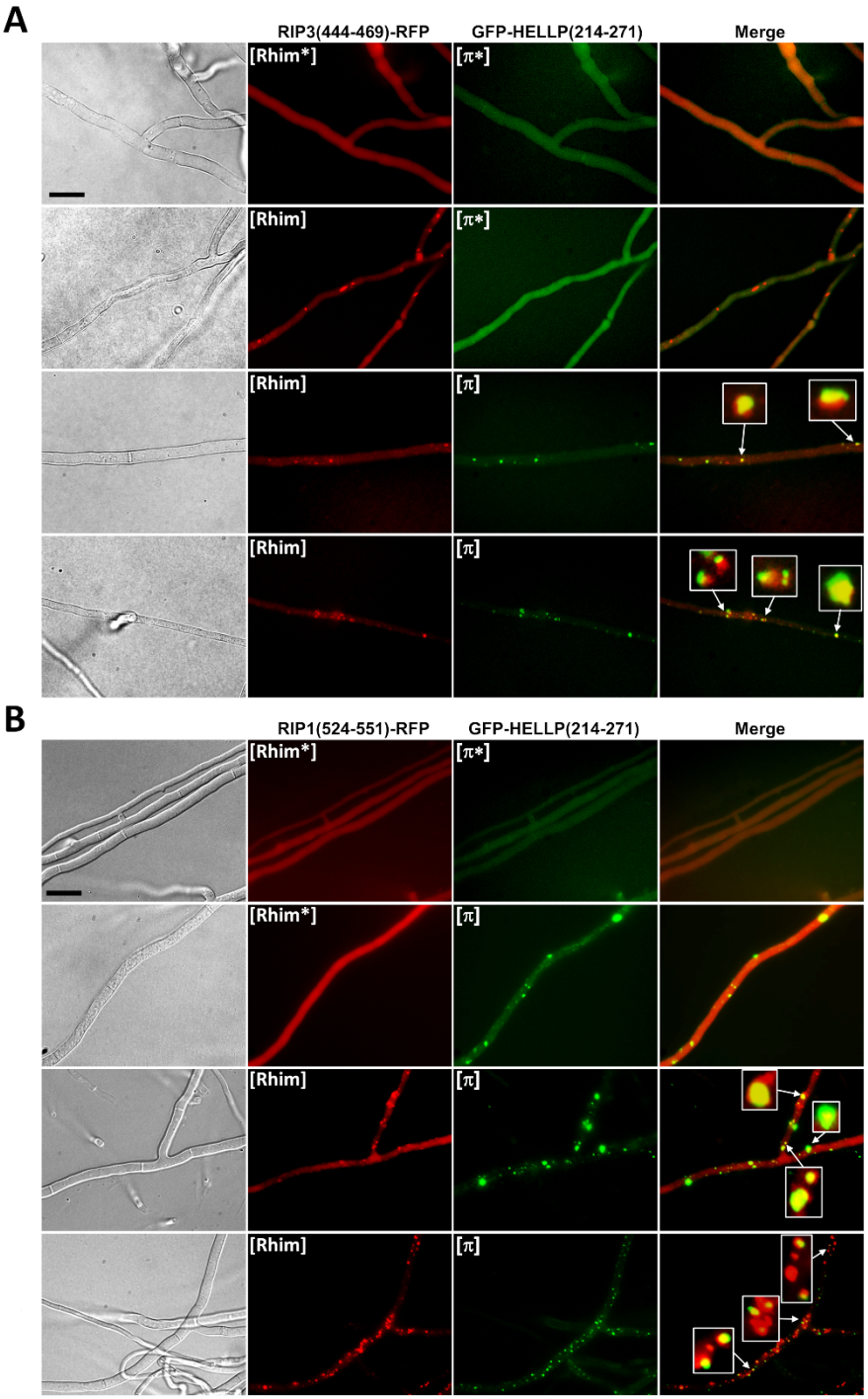

Fig 9. Partial cross-seeding *in vivo* between [π] and [Rhim] prions.

(A) Micrographs of strains co-expressing RIP3(444-469)-RFP ([Rhim*] or [Rhim] states) and GFP-HELLP(214-271) ([π*] or [π] states). (B) Micrographs of strains co-expressing RIP1(524-551)-RFP ([Rhim*] or [Rhim] states) and GFP-HELLP(214-271) ([π*] or [π] states). In both cases, note the co-existence in the second lane of [Rhim] and [π*] (A) or [Rhim*] and [π] (B), these

880 situations are only observable for a short period of time showing a low conversion rate of [π*]
881 by [Rhim] prion or of [Rhim*] by [π]. Note also the partial co-localization of the two prions,
882 some of the dots were zoomed to show incomplete overlapping in the case of heteropolymers
883 (Scale bar: 5 µm).

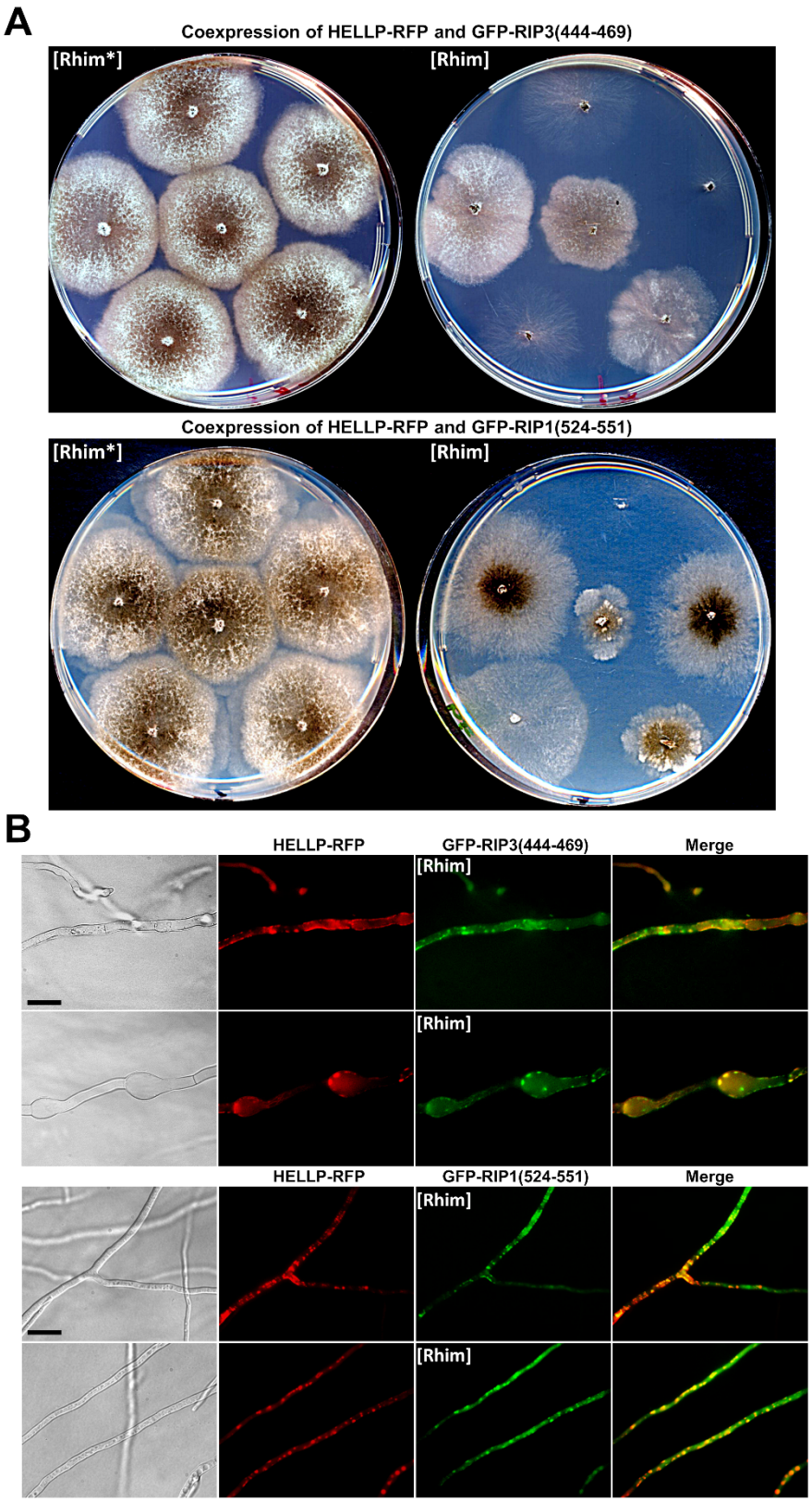

884

885 **Fig 10. Presence of [Rhim] prion elicits HELLP cell death activity *in vivo*.**

886 (A) Comparison of growth on solid medium of strains co-expressing HELLP-RFP and GFP-

887 RIP3(444-469) or RIP1(524-551) before and after contact with a [Rhim] prion containing strain.

888 Note that induction of [Rhim] spreading in transformants leads to altered growth phenotypes:
889 some of the transformants displayed drastic sublethal phenotypes and others only stunted
890 growth. (B) Micrographs of strains co-expressing full length HELLP-RFP and GFP-RIP3(444-469)
891 or GFP-RIP1(524-551) in the [Rhim] state. Note that HELLP relocalizes to the cell membrane in
892 presence of [Rhim] in dying cells or aggregates as dots partially co-localizing with [Rhim]
893 polymers in apparently more healthy cells.
894

895 **Supporting information captions**

896 **S1 Table. Monitoring of [π] prion propagation using barrage tests.**

897

898 **S2 Table. Test of the [Het-s] and [Φ] prions ability to convert [π*].**

899

900 **S3 Table. Test of cross-interactions between the three *P. anserina* amyloid signaling systems**

901 **by incompatibility assays.**

902 **S4 Table. [π] prion transmission and activation of HELLP or CgHELLP cell death activity across**

903 **the species barrier.**

904

905 **S5 Table. Cross-induction of HELLP and CgHELLP cell death activity by [π] prions.**

906

907 **S1 Fig. Homology between HeLo or HELL domains of *P. anserina* and pore forming domain**

908 **of human MLKL.**

909 (A) Alignment of the HET-S HeLo domain and the HELLF and HELLP HELL domains of *P. anserina*

910 with the 4HB region of the human MLKL. Alignment was generated with clustal omega with

911 default settings. As for CgHELLP, the first hit to HELLP is MLKL in HHPred searches with a p-

912 value score of $1.6x10^{-6}$ *versus* only $1.5 x10^{-4}$ for HET-S again emphasing its significant homology

913 with the MLKL 4HB necroptotic factor domain. (B) Secondary structure prediction for HELLP

914 HELL domain and MLKL 4HB domain using PSIPRED.

915

916 **S2 Fig. Observation of [π] prion propagation.**

917 (A) Micrographs of *P. anserina* strains expressing HELLP(171)271-GFP or GFP-HELLP(171-271)
918 as indicated above each micrograph (Scale bar: 5 µm). Transformants present initially a diffuse
919 fluorescence in the non-prion state designated [π*] (left) and acquire dot-like fluorescent
920 aggregates after contact with a strain already expressing the infectious prion state designated
921 [π] (right). (B) Barrage tests showing conversion of [π*] strains (expressing either HELLP(214-
922 271)-GFP or HELLP(171-271)-GFP) to [π] phenotype by contact with strains expressing GFP-
923 HELLP(214-271) in the [π] state. The acquired ability to form a barrage (marked by a white
924 arrow) with a tester strain expressing HELLP-GFP indicates conversion. [π] prion propagation
925 is allowed by the position of the inocula, as [π] and [π∗] strains are closer and made contact
926 before the tester strain reach the tested strain. A *Δhellp* strain was used as a negative control
927 of conversion.

928 **S3 Fig. HELLP full length diffuse and cytoplasmic localization.**

929 Micrographs of strains expressing HELLP-GFP or HELLP-RFP fusion proteins. The fluorescence
930 signal is diffuse and cytoplasmic and remains stable.

931

932 **S4 Fig. Lack of cross-seeding and co-localization *in vivo* between [π] and [Φ] prions.**

933 Micrographs of strains co-expressing HELLP(214-271)-RFP ([π*] or [π] state) and HELLF(209-
934 277)-GFP ([Φ*] or [Φ] state). Note an absence of co-localization of the two aggregated prion
935 forms ([Φ] and [π]) and the absence of conversion of [Φ*] state by [π] prion and of [π*] by [Φ]
936 prion.

937

938 **S5 Fig. Cross-seeding of [Rhim] prions in *P. anserina*.**

939 Micrographs of *P. anserina* strains coexpressing the molecular fusions RIP3(444-469)-RFP and
940 GFP-RIP1(524-551) or GFP-RIP3(444-469) and RIP1(524-551)-RFP. (Scale bar: 5 µm). Note the

941 strong colocalization between [Rhim] prions and dots alignment nearby the septa (zoomed
942 regions).
943
944 **S6 Fig. Partial cross-seeding of [π] and [Rhim] prions *in vivo*.**
945 (A) Micrographs of strains co-expressing GFP-RIP3(444-469) ([Rhim*] or [Rhim] states) and
946 HELLP(214-271)-RFP ([π*] or [π] states). (B) Micrographs of strains co-expressing GFP-
947 RIP1(524-551) ([Rhim*] or [Rhim] states) and HELLP(214-271)-RFP ([π*] or [π] states). In both
948 cases, note the co-existence on the second lane of [Rhim] and [π*] (A) or [Rhim*] and [π] (B),
949 these situations were only observable for a short period of time and showed a low conversion
950 rate of [π*] by [Rhim] prion or of [Rhim*] by [π]. Note the partial co-localization of the two
951 prions; some of the dots were zoomed to show incomplete overlapping. (C) Micrographs of
952 strains co-expressing GFP-RIP3(444-469) and RIP3(444-469)-RFP or GFP-RIP1(524-551) and
953 RIP1(524-551)-RFP of [Rhim] phenotypes. Note the almost complete overlapping of dots of
954 [Rhim] homopolymers (Scale bar: 5 μm).
955
956 **S7 Fig. Interaction between human RIP3 or RIP1 RHIM region and CgHELLP PFD.**
957 (A) Induction of [Rhim] prion by cross conversion of [Rhim*] by [π] Cg or [Rhim] prions.
958 Histogram representing the percentage of [Rhim*] strains displaying [Rhim] phenotype after
959 contact with a *Δhellp Δhet-s Δhellf* prion free strain (control), a GFP-CgHELLP(215-278) [π]
960 containing strain or a GFP-RIP3(444-469) or GFP-RIP1(524-551) [Rhim] containing strains
961 (indicated on top). Strains phenotype after induction was determined by monitoring the
962 acquisition of dot-like aggregates by fluorescence microscopy. Percentages of prion formation
963 were expressed as the mean value ± standard deviation for 3 to 5 independent experiments
964 on 4 different transformants. P-values for cross conversion were determined using two tails

965 Fisher's test by comparison of the number of prion free and prion containing strains obtained
966 after induction by the prion free control or by the heterotypic prion containing strain. (B)
967 Partial cross-seeding of [π] Cg and [Rhim] prions *in vivo*. Micrographs of strains co-expressing
968 RIP3(444-469)-RFP or RIP1(524-551)-RFP ([Rhim*] or [Rhim] states) and GFP-CgHELLP(215-
969 278) ([π∗] and [π] state). Note the co-existence of [Rhim*] and [π], this situation is only
970 observable for a short period of time, showing a low conversion rate of [Rhim*] by [π] prion.
971 Note the partial co-localization of the two prions, some of the dots were zoomed to show
972 incomplete overlapping (Scale bar: 5 μm).

973 **S8 Fig. Cell death occurring throughout confrontation of [Rhim] and HELLP expressing**
974 **strains.**

975 Micrographs showing confrontations between HELLP-GFP and GFP-RIP3(444-469) (Upper
976 panel) or GFP-RIP1(524-551) (lower panel) expressing strains after Evans blue staining. Note
977 that heterocaryotic fusion cells are stained indicating their death. Scale bar (2 μm).

978

979 **S9 Fig. Triggering of CgHELLP cell death activity *in vivo* by [Rhim] prion**

980 (A) Growth of strains co-expressing CgHELLP-RFP and GFP-RIP3(444-469) or GFP-RIP1(524-
981 551) before and after contact with a [Rhim] prion containing strain were compared on solid
982 medium. Note that induction of [Rhim] in transformants leads to growth alteration to varying
983 extent ranging from sublethal phenotype to more or less stunted growth. (B) Micrographs of
984 strains co-expressing full length CgHELLP-RFP and GFP-RIP3(444-469) or GFP-RIP1(524-551) in
985 the [Rhim] state. CgHELLP relocalizes to the cell membrane or aggregates as dots partially co-
986 localizing with [Rhim] polymers in damaged cells (Scale bar: 5 μm).

987

988